

New Generation of Parton Distributions with Uncertainties from Global QCD Analysis

J. Pumplin, D.R. Stump, J. Huston, H.L. Lai*, P. Nadolsky†, W.K. Tung

*Department of Physics and Astronomy
Michigan State University
East Lansing, MI 48824 USA*

ABSTRACT: A new generation of parton distribution functions with increased precision and quantitative estimates of uncertainties is presented. This work significantly extends previous CTEQ and other global analyses on two fronts: (i) a full treatment of available experimental correlated systematic errors for both new and old data sets; (ii) a systematic and pragmatic treatment of uncertainties of the parton distributions and their physical predictions, using a recently developed eigenvector-basis approach to the Hessian method. The new gluon distribution is considerably harder than that of previous standard fits. A number of physics issues, particularly relating to the behavior of the gluon distribution, are addressed in more quantitative terms than before. Extensive results on the uncertainties of parton distributions at various scales, and on parton luminosity functions at the Tevatron RunII and the LHC, are presented. The latter provide the means to quickly estimate the uncertainties of a wide range of physical processes at these high-energy hadron colliders, based on current knowledge of the parton distributions. In particular, the uncertainties on the production cross sections of the W, Z at the Tevatron and the LHC are estimated to be $\pm 4\%$ and $\pm 5\%$ respectively, and that of a light Higgs at the LHC to be $\pm 5\%$.

KEYWORDS: parton distribution functions, quantum chromodynamics.

*Current address: Ming-Hsin Institute of Technology, Hsin-Chu, Taiwan

†Current address: Department of Physics, Southern Methodist University, Dallas, Texas 75275-0175

Contents

1. Introduction	2
2. New Input and Methodology	3
2.1 Experimental Data Sets	3
2.2 χ^2 Function and Treatment of Correlated Systematic Errors	3
2.3 Methods for Analysis of Uncertainties	5
2.4 Perturbative QCD Parameters and Input	6
2.5 Parametrization of Nonperturbative Input PDF's	7
3. Results on New Parton Distributions	8
3.1 The New Standard PDF Sets	8
3.1.1 Comparison with Data	9
3.1.2 The New Parton Distributions in the \overline{MS} scheme	13
3.1.3 DIS and LO Parton Distributions	14
3.2 Eigenvector PDF Sets For Uncertainty Analyses	15
3.2.1 Uncertainties of PDF's	16
3.3 Issues And Comments	18
3.3.1 How much progress has been made?	18
3.3.2 Higher twist terms?	19
3.3.3 Signs of anomalies at large x or small x ?	20
3.3.4 Determination of α_s ?	21
3.4 User Interface	22
4. Physical Predictions and their Uncertainties	22
5. Comparison with Other Parton Distribution Analyses	24
5.1 Previous Uncertainty Studies	24
5.2 Comparison to MRST2001	25
6. Concluding Remarks	28
A. Details of the CTEQ6M fit	30
B. Comparison of Theory and Data with Correlated Errors	30
B.1 Useful formulas for χ^2 and the analysis of systematic errors	31
B.2 Useful tools for evaluating fits and interpreting results	32
B.3 Error analysis of DIS data	33
B.4 The tolerance criterion	35
C. Study of Higher Twist Effects	38

1. Introduction

Progress on the determination of the parton distribution functions (PDF’s) of the nucleon, from global quantum chromodynamics (QCD) analysis of hard scattering processes, is central to precision standard model (SM) phenomenology, as well as to new physics searches, at lepton-hadron and hadron-hadron colliders. There have been many new developments in recent years, beyond the conventional analyses that underlie the widely used PDF’s [1–3]. These developments have been driven by the need to quantify the uncertainties of the PDF’s and their physical predictions [4–12]. We report in this paper on a comprehensive new global QCD analysis based on the most current data, and on the recently developed methods of uncertainty study of [10–12]. This new analysis includes a full treatment of all available correlated experimental errors, as well as an extensive exploration of the parametrization of the input nonperturbative PDF’s.

Although this work is built on the series of previous CTEQ parton distributions [2], it represents more than an evolutionary updating of previous work to incorporate new experimental data sets. The methodology of [10–12] goes beyond the traditional paradigm of producing some subjectively chosen “best fits.” It introduces a set of efficient and practical tools to characterize the parton parameter space in the neighborhood of the global minimum. This allows the systematic exploration of the uncertainties of parton distributions and their physical predictions due to known experimental errors and due to the input theoretical model parameters.

There are many complex issues involved in a comprehensive global parton distribution analysis. Foremost among these on the experimental side is the “imperfection” of real experimental data compared to textbook behavior—for instance, some experimental measurements appear to be statistically improbable because the χ^2 / N deviates from 1 substantially more than the expected $\pm\sqrt{2/N}$; or different precision experimental measurements of the same physical quantities appear to be statistically incompatible in all regions of the model parameter space. The methods of [10–12] cannot resolve these problems—no global analysis method can—but the tools developed in this formalism make it possible to look deeper into some of these problems, in order to assess the acceptability and compatibility of the affected data sets in more practical terms, and to suggest pragmatic ways to deal with the apparent difficulties. These detailed studies were not possible in the conventional analyses [1–3] and [13]. On the theoretical side, the uncertainties on the perturbative QCD (PQCD) calculations of the various physical processes included in the global analysis are not easily quantified in a uniform way. We do not address that problem here.

Section 2 summarizes the experimental and theoretical input to the global analysis, emphasizing the new elements in data sets and in methodology. Section 3 presents results on the new generation of PDF’s: the “standard” CTEQ6 sets, as well as the eigenvector

sets that characterize the uncertainties. It also includes discussions of various physics issues relating to these global fits. Section 4 presents some general results on uncertainties of physics predictions due to PDF's, in the form of parton-parton luminosity functions for the Tevatron RunII and for the LHC. Section 5 compares this work to previous studies of PDF uncertainties [4–7] (primarily on DIS experiments), and to a recent general PDF analysis [13]. Four appendices concern: (A) detailed information on the new standard parton distribution set CTEQ6M; (B) new formulas and tools for understanding the significance of χ^2 values for individual experiments and estimating ranges of uncertainties in the comparison of fits with data; (C) assessing the need for higher-twist (power-law) contributions to the theory model; and (D) studying the impact of the flexibility associated with the choice of parametrization for the nonperturbative PDF's.

2. New Input and Methodology

The next-to-leading order (NLO) global QCD analysis carried out in this work is built on the same basis as the previous CTEQ parton distribution sets [2]. In this section, we describe the new experimental input and the new theoretical techniques, which together have enabled substantial progress in this generation of global analysis.

2.1 Experimental Data Sets

Since the CTEQ5 analysis, many new experimental data sets have become available for an improved determination of parton distributions. Particularly noteworthy are the recent neutral current deep-inelastic scattering (DIS) structure function measurements of H1 [14] and ZEUS [15], and the inclusive jet cross section measurement of DØ [16] (in several rapidity bins, up to a rapidity of 3). The greater precision and expanded (x, Q) ranges compared to previous data in both processes provide improved constraints on the parton distributions. Other recent data used in the analysis are the updated E866 measurements of the Drell-Yan deuteron/proton ratio [17] and the re-analyzed CCFR measurement of F_2 [18].

These new results complement the fixed-target DIS experiments of BCDMS [19, 20], NMC [21], CCFR F_3 [22], the Drell-Yan measurement of E605 [23], the CDF measurement of W -lepton asymmetry [24], and the CDF measurement of inclusive jets [25], which this study shares with the earlier CTEQ5 analysis. Even for these older experiments, our new analysis, by including correlated systematic errors (cf. Sec. 2.2 and Appendix B.1), incorporates more details than previous [1, 2] and recent [13] analyses. For instance, for the BCDMS and NMC experiments we now use the data sets measured at separate energies (which contain full information on correlated errors) instead of the combined data sets (which, due to re-binning of data points, retain only some effective point-to-point uncorrelated errors of uncertain statistical significance).

2.2 χ^2 Function and Treatment of Correlated Systematic Errors

The very extensive and precise DIS data from fixed-target and HERA experiments provide the backbone of parton distribution analysis. In order to make full use of the experimental

constraints, it is important to incorporate the available information on correlated systematic errors [4–7, 10–12]. The same is true for recent data on inclusive jets [16, 25], where the experimental uncertainties are dominated by systematics. Thus, for the first time in the CTEQ series of analyses, we have included the correlated errors wherever available. Our analysis is simplified by a novel way of treating systematic errors, formulated in [12] (cf. also the recent review [26]). As an introduction to subsequent discussions based on this method, we mention its basic ideas and main features here. A more complete summary of this method is given in Appendix B.1, as needed to explain the detailed comparison between data and fits discussed in that section.

In global fits not including correlated errors, one would minimize a naive global χ^2 function defined simply as $\chi_0^2 = \sum_{\text{expt.}} \sum_{i=1}^{N_e} (D_i - T_i)^2 / \sigma_i'^2$, where N_e is the number of data points in experiment e , D_i is a data value, T_i is the corresponding theory value (which depends on the PDF model), and $\sigma_i'^2 = \sigma_i^2 + \Sigma_i^2$ is the statistical (σ_i^2) and point-to-point systematic (Σ_i^2) errors added in quadrature. The function χ_0^2 provides the simplest means to search for candidates of “good” global fits, but has rather limited use in assessing uncertainties of the resulting fits.

If there are K sources of correlated systematic errors, specified by standard deviations $\{\beta_{1i}, \beta_{2i}, \dots, \beta_{Ki}\}$, in addition to an uncorrelated systematic error u_i for data point i , then a standard method to improve the treatment of experimental errors is to construct the covariance matrix $V_{ij} = \alpha_i^2 \delta_{ij} + \sum_{k=1}^K \beta_{ki} \beta_{kj}$, from which a global χ^2 function is defined by $\chi^2 = \sum_{\text{expt.}} \sum_{i,j=1}^{N_e} (D_i - T_i) V_{ij}^{-1} (D_j - T_j)$. (Here $\alpha_i^2 = \sigma_i^2 + u_i^2$.) An alternative method is to add K parameters, each associated with one systematic error, and to minimize an *extended* χ^2 function with respect to the combined set of experimental and theoretical parameters (denoted by χ'^2 in Appendix B.1, Eq. (B.2)). These well-known methods are equivalent. Both face some practical, even formidable, problems in the context of global QCD analysis because of the large number of data points (which can make the inversion of the covariance matrix numerically unstable) and the large number of fitting parameters (which becomes unmanageable when all systematic errors from all experiments are included).

The method formulated in [12] overcomes these difficulties by solving the problem of optimization with respect to the correlated systematic errors analytically. The result is an effective χ^2 minimization problem with respect to only the theory parameters, as for the simple case. The resulting χ^2 function has the form (cf. Eq. (B.5)):

$$\chi^2 = \sum_{\text{expt.}} \left\{ \sum_{i=1}^{N_e} \frac{(D_i - T_i)^2}{\alpha_i^2} - \sum_{k,k'=1}^{K_e} B_k (A^{-1})_{kk'} B_{k'} \right\}, \quad (2.1)$$

where $\{B_k\}$ is a K_e -component vector, $\{A_{kk'}\}$ is a $K_e \times K_e$ matrix, and

$$B_k = \sum_{i=1}^{N_e} \frac{\beta_{ki} (D_i - T_i)}{\alpha_i^2}, \quad A_{kk'} = \delta_{kk'} + \sum_{i=1}^{N_e} \frac{\beta_{ki} \beta_{k'i}}{\alpha_i^2}. \quad (2.2)$$

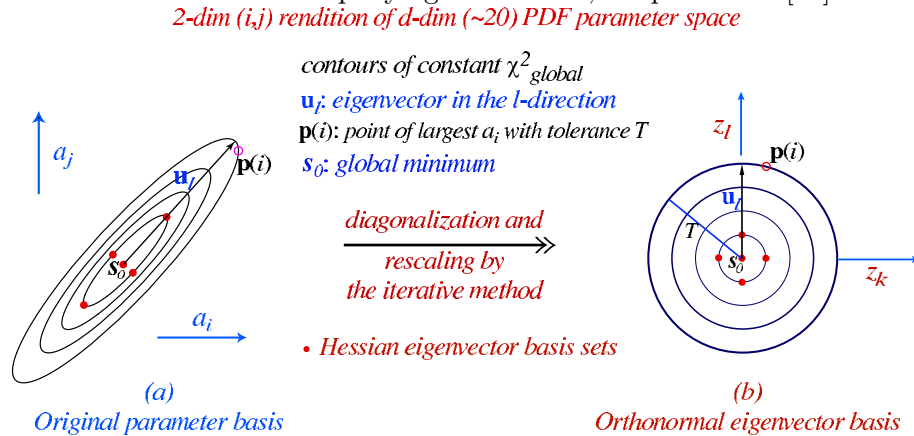
Not only is the matrix inversion simpler and more stable ($K_e \times K_e$ with $K_e \leq 10$, compared to $N_e \times N_e$ with N_e as large as 300, in the correlation matrix approach), the explicit formula

for the contribution of the various sources of systematic errors in Eq. (2.1) provides a useful tool to evaluate the uncertainties in detailed analysis of the fits—as explained in Appendix B.1 and used in discussions in subsequent sections—which is not available in the traditional approach.

2.3 Methods for Analysis of Uncertainties

The widely used parton distributions [1–3, 13] are obtained from global analyses using a “best-fit” paradigm, which selects the *global minimum* of the chosen χ^2 function. However, the “best” PDF’s are subject to various uncertainties. Within this paradigm, the problem of estimating uncertainties of the PDF’s can only be addressed in an *ad hoc* manner, usually by examining alternative fits obtained by subjective tuning of selected degrees of freedom. Recent efforts to assess the uncertainties objectively, using established statistical methods, have been mostly concerned with the precision DIS experimental data [4–7], rather than the global analysis of all hard scattering data. As mentioned in the introduction, there are formidable complications when standard statistical methods are applied to global QCD analysis. The basic problem is that a large body of data from many diverse experiments,¹ which are not necessarily compatible in a strict statistical sense, is being compared to a theoretical model with many parameters, which has its own inherent theoretical uncertainties.

In recent papers [10–12], we have formulated two methods, the Hessian and the Lagrange, which overcome a number of long-standing technical problems encountered in applying standard error analysis to the complex global analysis problem. We are now able to characterize the behavior of the χ^2 function in the *neighborhood* of the global minimum in a reliable way. This provides a systematic method to assess the compatibility of the data sets in the framework of the theoretical model [27], and to estimate the uncertainties of the PDF’s and their physical predictions within a certain practical tolerance. The basic ideas are summarized in the accompanying illustration, adapted from [11]:



The behavior of the global χ^2 function in the neighborhood of the minimum in the PDF parameter space is encapsulated in $2N_p$ sets of eigenvector PDF’s (where $N_p \sim 20$ is the

¹For our analysis, there are ~ 1800 data points from ~ 15 different sets of measurements with very different systematics and a wide range of precision.

number of free PDF parameters), represented by the solid dots in the illustration. These eigenvectors are obtained by an iterative procedure to diagonalize the Hessian matrix, adjusting the step sizes of the numerical calculation to match the natural physical scales. This procedure efficiently overcomes a number of long-standing obstacles² encountered when applying standard tools to perform error propagation in the global χ^2 minimization approach. Details are given in [10, 11].

The uncertainty analysis for our new generation of PDF's makes full use of this method. The result is $2N_p + 1$ PDF sets, consisting of the best fit S_0 and eigenvector basis sets in the plus and minus directions along each eigenvector. From these PDF sets we can calculate the best estimate, and the range of uncertainty, for the PDF's themselves and for any physical quantity that depends on them. The uncertainty can be computed from the simple master formula

$$\Delta X = \frac{1}{2} \left(\sum_{i=1}^{N_p} [X(S_i^+) - X(S_i^-)]^2 \right)^{1/2}, \quad (2.3)$$

where X is the observable, and $X(S_i^\pm)$ are the predictions for X based on the PDF sets S_i^\pm from the eigenvector basis.

2.4 Perturbative QCD Parameters and Input

The fundamental parameters of perturbative QCD are the coupling α_s and the quark masses. In principle, these parameters can be determined in the global fit, along with the nonperturbative parton distribution functions. In practice, they are determined more precisely and definitively in dedicated measurements. We therefore treat these parameters as input to our global analysis. For α_s , we use $\alpha_s(M_Z) = 0.118$, the Particle Data Group average [28]. (However, cf. the discussion on leaving α_s free in the fitting in Sec. 3.3.4 and Sec. 5.2.) The light quarks u, d, s are treated as massless, as usual. In the \overline{MS} scheme, the evolution kernels of the PDF's are mass-independent: charm and bottom masses enter only through the scales at which the heavy quark flavors are turned on in the evolution. We take $m_c = 1.3$ GeV and $m_b = 4.5$ GeV.

The hard matrix elements that enter into the PQCD calculations are all taken to be at NLO (except for the LO fit, of course). Although it is now possible to incorporate charm and bottom mass effects in the NLO hard cross sections, in the so-called variable flavor number scheme (VFNS) [29–32], we have decided to use the conventional (zero-mass parton) hard cross sections in our standard analysis for three practical reasons. First, hard cross-section calculations in the VFNS (with non-zero parton masses) are not yet available for processes other than DIS. Second, even in DIS, there are different ways to implement the VFNS. This introduces yet another type of “scheme dependence”, and hence a source of confusion for users of PDF's. (A recently proposed “natural” implementation of the VFNS [33], if widely accepted, could alleviate this source of confusion.) Finally, since most

²The obstacles are due to difficulties in calculating physically meaningful error matrices by finite differences, in the face of (i) vastly different scales of eigenvalues ($\sim 10^7$) in different, a priori unknown, directions in the high-dimension parameter space, and (ii) numerical fluctuations due to (multi-dimensional) integration errors in the theoretical (PQCD) calculation and round-off errors.

users of PDF’s only have at their disposal the standard hard cross sections for zero-mass partons, it is preferable to have PDF’s determined by a global analysis calculated in the same way as they are used. In a subsequent paper, we will study the heavy quark mass effects in global analysis in detail, and publish PDF’s determined in the VFNS with a full treatment of quark mass effects, using the natural implementation of [33].

2.5 Parametrization of Nonperturbative Input PDF’s

The nonperturbative input to the global analysis are PDF’s specified in a parametrized form at a fixed low-energy scale $Q_0 = 1.3 \text{ GeV}$.³ The particular functional forms, and the value of Q_0 , are not crucial, as long as the parametrization is flexible enough to describe the range of behavior permitted by the available data at the level of accuracy of the data. Intuitive notions of smoothness may be built into the input functions. The PDF’s at all higher Q are determined from the input functions by the NLO perturbative QCD evolution equations.

The functional form that we use is

$$x f(x, Q_0) = A_0 x^{A_1} (1 - x)^{A_2} e^{A_3 x} (1 + e^{A_4} x)^{A_5} \quad (2.4)$$

with independent parameters for parton flavor combinations $u_v \equiv u - \bar{u}$, $d_v \equiv d - \bar{d}$, g , and $\bar{u} + \bar{d}$. We assume $s = \bar{s} = 0.2(\bar{u} + \bar{d})$ at Q_0 . The form (2.4) is “derived” by including a 1:1 Padé expansion in the quantity $d[\log(xf)]/dx$. This logarithmic derivative has an especially simple form for the time-honored canonical parametrization $x f(x) = A_0 x^{A_1} (1 - x)^{A_2}$. For our parametrization there are poles at $x = 0$ and $x = 1$ to represent the singularities associated with Regge behavior at small x and quark counting rules at large x , along with a ratio of (linear) polynomials to describe the intermediate region in a smooth way.

Equation (2.4) provides somewhat more versatility than previous CTEQ parametrizations. For some flavors, it has more freedom than needed, so that not all of the parameters can be determined by the present data. In those cases, some parameters are held fixed, guided by the Hessian method in the final fitting process as discussed in Sec. 3.2 and in Ref. [11]. In the future, more data may find even this parametrization too restrictive—first for the very well constrained $u(x)$ —and it will be natural to proceed to a 2:2 Padé form. To distinguish the \bar{d} and \bar{u} distributions, we parametrize the *ratio* \bar{d}/\bar{u} , as a sum of two terms:

$$\bar{d}(x, Q_0)/\bar{u}(x, Q_0) = A_0 x^{A_1} (1 - x)^{A_2} + (1 + A_3 x) (1 - x)^{A_4} . \quad (2.5)$$

Altogether we use 20 free shape parameters to model the PDF’s at Q_0 .

An extensive study of the sensitivity of the global fits to the choice of parametrization has been carried out in the process of this analysis, by trying different parametrizations, and

³In CTEQ5 and other recent global fits, the slightly lower value $Q_0 = 1 \text{ GeV}$ was used. Because QCD evolution is quite rapid in the $Q \sim 1\text{--}2 \text{ GeV}$ range, one gets enhanced sensitivity to the parameters when starting from a relatively low scale. However, that rapid variation, which occurs below the region of applicability of PQCD, can produce unusual behavior of the functions at small Q , which may have no *physical* significance. Cf. the discussions in Sec. 5.2 and Appendix D.

by using different values of Q_0 (which is equivalent to changing the functional forms). In the main body of this paper, we concentrate on results obtained with the standard choices described above. Comments on the effects of parametrization on the physics results will be made in the text as appropriate. Some studies of results obtained with alternative parametrizations are described in Appendix D.

3. Results on New Parton Distributions

With the theoretical and experimental input, methods, and parametrizations described above, we arrive at a *standard set* of parton distributions (the nominal “best fit”) together with a *complete set of eigenvector parton distribution sets* that characterizes the neighborhood of acceptable global fits in the parton parameter space. The study is carried out mainly in the \overline{MS} scheme.⁴ We now discuss the salient features of the results and the related physics issues.

3.1 The New Standard PDF Sets

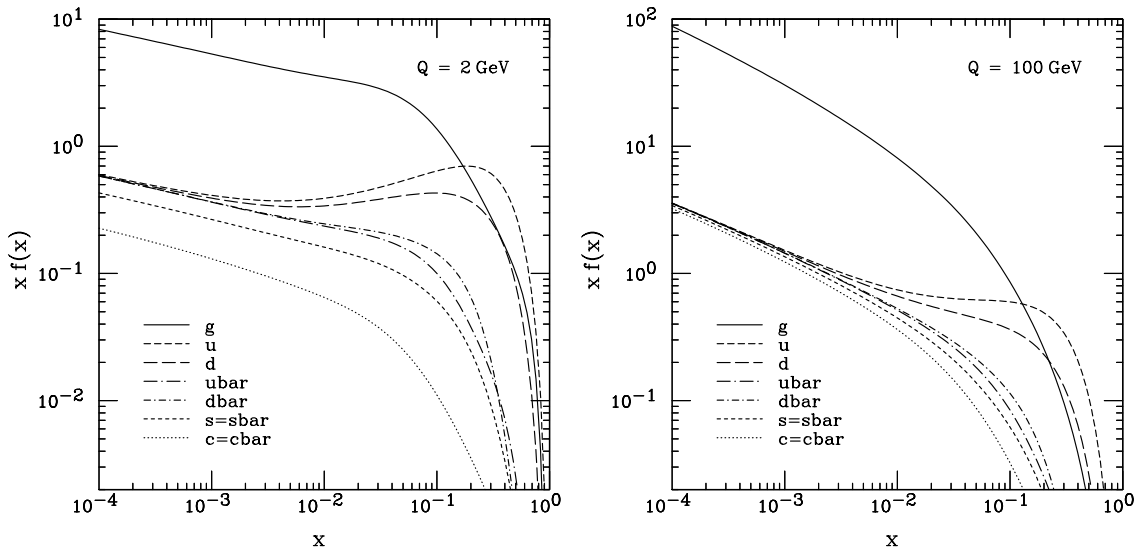


Figure 1: Overview of the CTEQ6M parton distribution functions at $Q = 2$ and 100 GeV.

The standard set of parton distributions in the \overline{MS} scheme, referred to as CTEQ6M, provides an excellent global fit to the data sets listed in Sec. 2.1. An overall view of these PDF’s is shown in Fig. 1, at two scales $Q = 2$ and 100 GeV. The overall χ^2 for the CTEQ6M fit is 1954 for 1811 data points. The parameters for this fit and the individual χ^2 values for the data sets are given in Appendix A. In the next two subsections, we discuss the comparison of this fit to the data sets, and then describe the new features of the parton distributions themselves. Quantitative comparison of data and fit is studied in more depth in Appendix B.

⁴For the convenience of certain applications, we also present one standard set each of parton distributions in the DIS scheme and at leading order. Cf. Sec. 3.1.3.

3.1.1 Comparison with Data

The fact that correlated systematic errors are now fully included in the fitting procedure allows a more detailed study of the quality of fits than was possible in the past. We can take the correlated systematic errors into account explicitly when comparing data and theory, by using the procedure discussed in Sec. B.2 of Appendix B. In particular, based on the formula for the extended χ^2 function expressed in the simple form Eq. (B.6), we obtain a precise graphical representation of the quality of the fit by superimposing the theory curves on the shifted data points $\{\widehat{D}_i\}$ containing the fitted systematic errors. The remaining errors are purely uncorrelated, hence are properly represented by error bars. We use this method to present the results of our fits whenever possible.

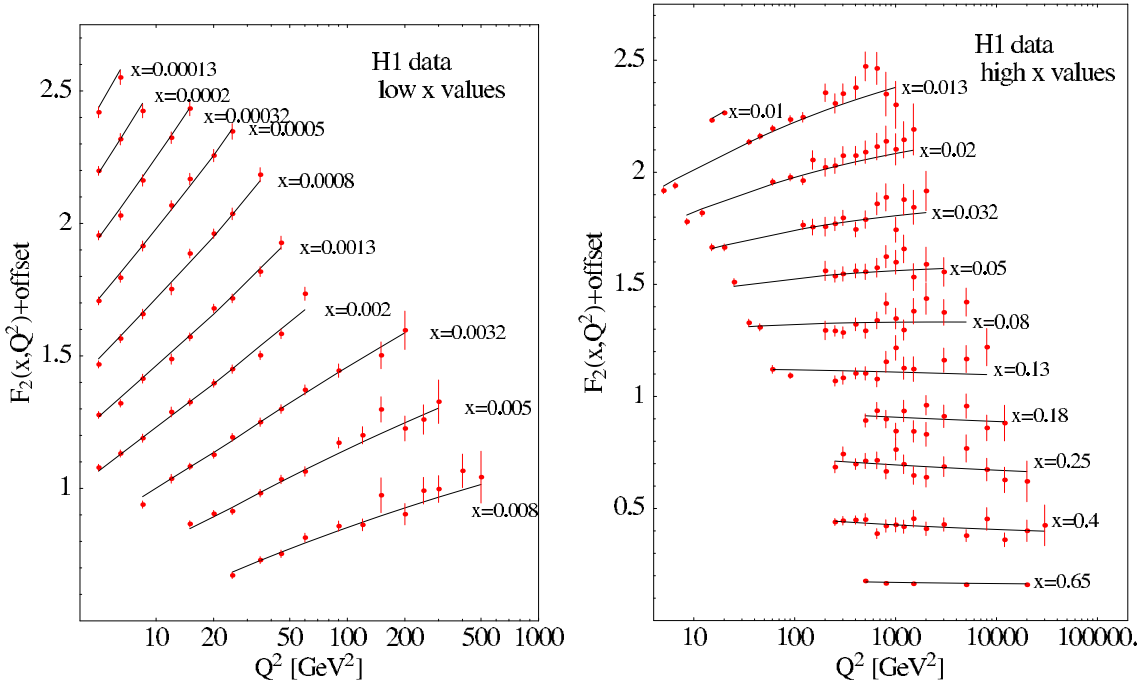


Figure 2: Comparison of the CTEQ6M fit to the H1 data [14] in separate x bins. The data points include the estimated corrections for systematic errors. The error bars contain statistical only.

Figure 2 shows the comparison of the CTEQ6M fit to the latest data of the H1 experiment [14]. The extensive data set is divided into two plots: (a) for $x < 0.01$, and (b) for $x > 0.01$. In order to keep the various x bins separated, the values of F_2 on the plot have been offset vertically for the k th bin according to the formula: ordinate = $F_2(x, Q^2) + 0.15k$. The excellent fit seen in the figure is supported by a χ^2 value of 228 for 230 data points. Similarly, Fig. 3 shows the comparison to the latest data from ZEUS [15]. One again sees very good overall agreement. The χ^2 value is 263 for 229 data points. This is 2σ ($\sigma = \sqrt{2N} = 21$) away from the ideal value of $N = 229$. A closer inspection of Fig. 3 does not suggest any systematic disagreement. To assess the significance of this 2σ effect, we examine in detail the systematic shifts obtained in the fit in Appendix B.3. We find

that they are all quite reasonable, thus giving us confidence that the fit is indeed of good quality.

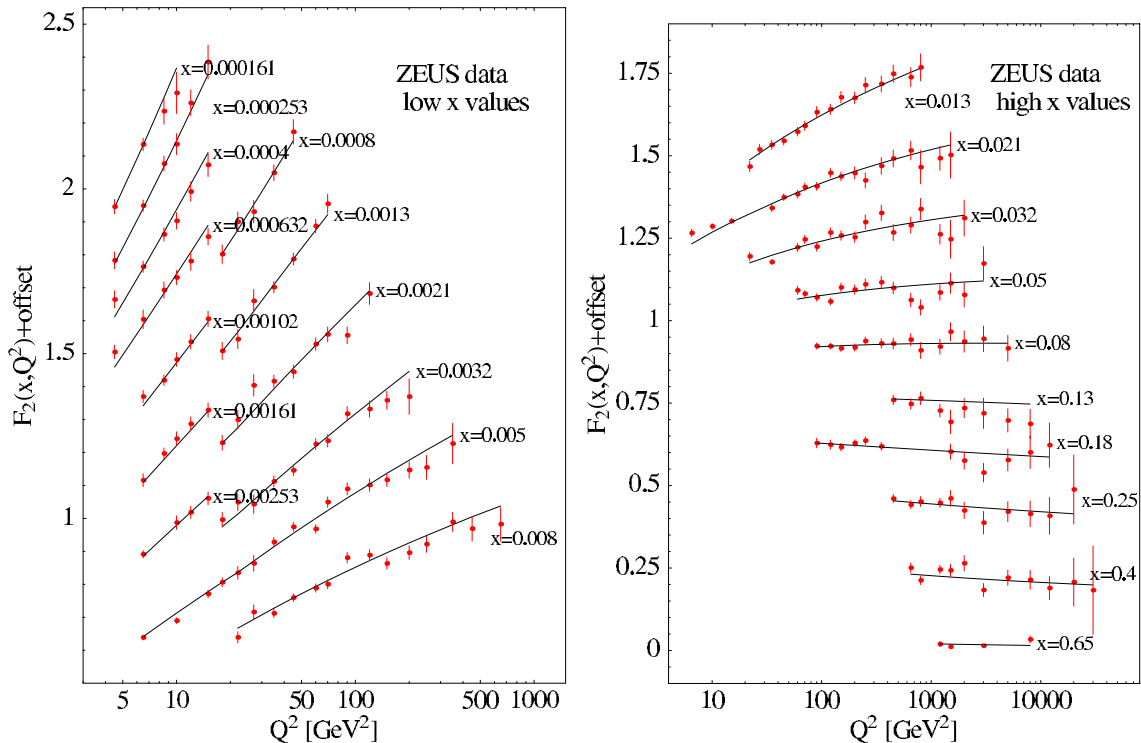


Figure 3: Comparison of the CTEQ6M fit to the ZEUS data [15]. Same format as Fig. 2.

The new PDF’s also fit the older fixed-target DIS experiments well—similar to previous global analyses. Figure 4 shows the comparison to the fixed-target neutral current experiments BCDMS and NMC. Because we are incorporating the fully correlated systematic errors, the data sets used for these experiments are those obtained at each measured incoming energy, rather than the “combined” data sets that are usually shown. This more detailed and quantitative comparison is important when we try to evaluate the statistical significance of the fits in our uncertainty analysis (cf. Appendix B). The χ^2 per data point for these data sets are 1.11 (378/339) for BCDMS and 1.52 (305/201) for NMC. The fit to the BCDMS data is clearly excellent, both by inspection of Fig. 4a and by the normal χ^2 test. For the NMC data, Fig. 4b shows rather good overall agreement, but with some notable large fluctuations away from the smooth theory curves. The most noticeable fluctuations—points with almost the same (x, Q) values—are from data sets taken at different incoming energies.⁵ This is reflected in the χ^2 value which is quite a bit larger than expected for a normal probability distribution. This raises two issues: (i) Is the fit acceptable or unacceptable? (ii) Can the fit be substantially improved by a different theoretical model, e.g., the inclusion of higher-twist terms? The first question is addressed in Sec. B.3,

⁵These fluctuations are smoothed out by re-binning and other measures in the combined data set [21], which is not used here.

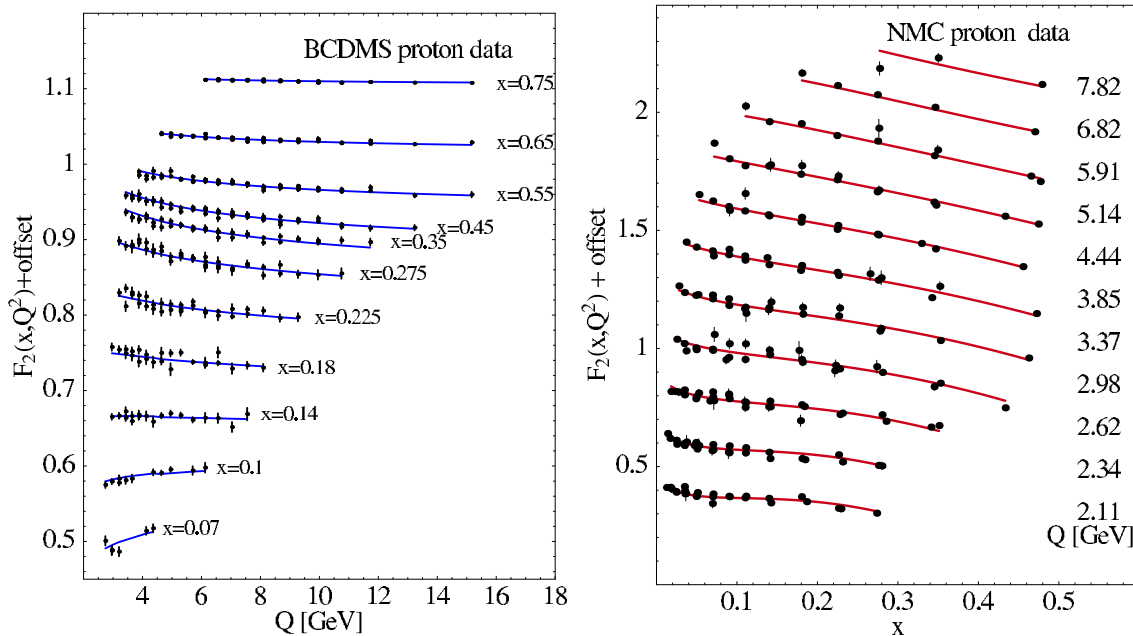


Figure 4: Comparison of the CTEQ6M fit with the BCDMS [19] and NMC [21] data on μp DIS. Same format as Fig. 2. (The offset for the k th Q value in (b) is $0.2k$.)

where the excess χ^2 is shown to be attributable to larger-than-normal fluctuations of the data points (which is unrelated to the viability of the theory model), and that the shifts due to systematic errors (which is related to the goodness-of-fit) are all within the range of normal statistics. The second question is addressed in Sec. 3.3.2 and Appendix C, where we show that the inclusion of higher-twist contributions does not result in a substantial improvement of the fit.

The charged-current DIS data from the CCFR experiment are also used in our global analysis. The agreement between data and theory for the CCFR measurements of F_2 and F_3 is good, comparable to previous analyses. Because of the important role of the charm quark in the quantitative treatment of this process, and the lack of information on correlations between the current F_2 and F_3 data,⁶ we defer a detailed study of the charged-current DIS fit to the forthcoming global analysis including heavy quark mass effects.

Of the new experimental input, perhaps the most interesting and significant in its impact on the parton distributions is the one-jet inclusive cross section from DØ [16]. These new data represent a considerable expansion in kinematic range over the previous jet measurements, by providing measurements in 5 separate rapidity bins, with η up to 3.0. Our fits agree extremely well with these data, in both shape and magnitude over the full kinematic range, as shown in Fig. 5a. Comparison to the corresponding CDF measurement in the central rapidity region is also shown in the parallel plot, Fig. 5b.

The agreement between theory and experiment is made even clearer in Fig. 6 where

⁶The CCFR F_2 measurements have been re-analyzed in a model-independent way [18]. The new data are presented in a such a way that correlations with the old F_3 measurements [22] are no longer available.

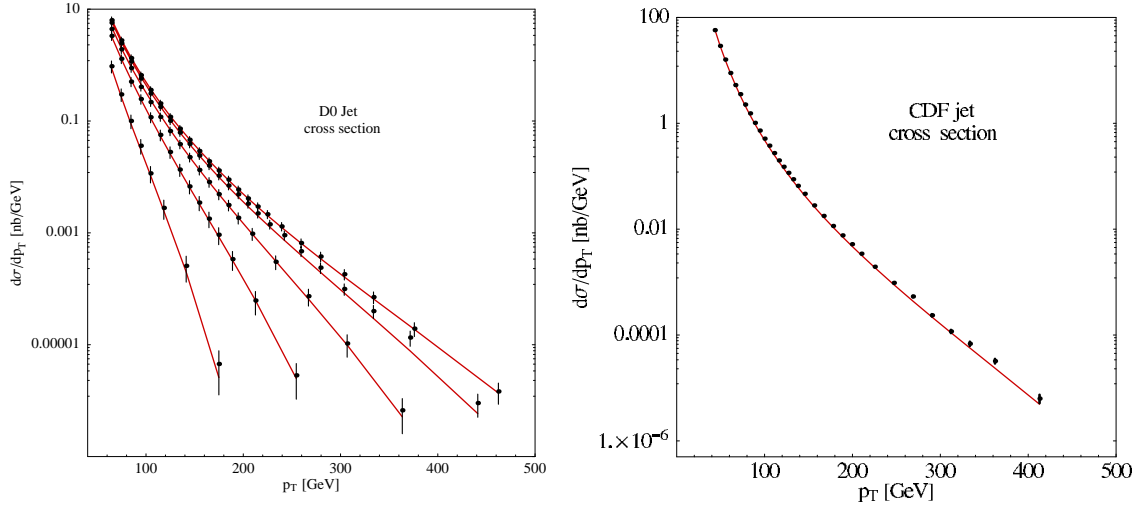


Figure 5: Comparison of the CTEQ6M fit to the inclusive jet data. (a) DØ (the boundary values of the 5 rapidity bins are 0, 0.5, 1.0, 1.5, 2.0 and 3.0) [16]; (b) CDF (central rapidity, $0.1 < |\eta| < 0.7$) [25].

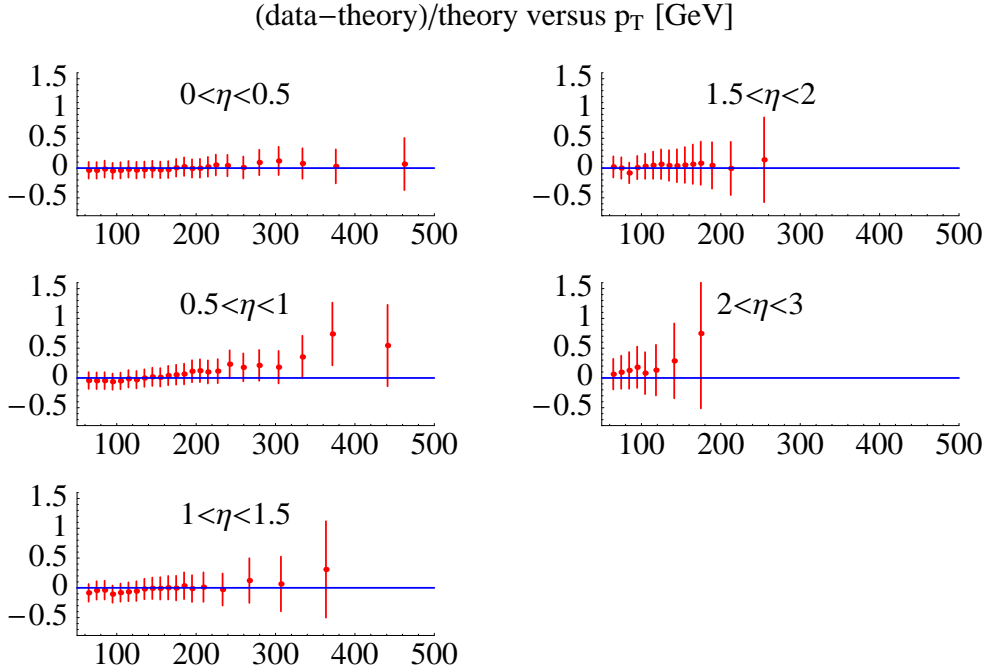


Figure 6: Closer comparison between CTEQ6M and the DØ jet data as fractional differences.

the difference between data and theory is plotted. The χ^2 value for the fit to the jet data, including all systematics, is 118/123, combining the two experiments. In Figs. 5 and 6, the error bars are combined statistical and diagonal systematic errors.⁷ The ratio plot

⁷The DØ jet data involve partially correlated systematic errors which can only be characterized by a

comparing to the CDF data is not shown; it is similar to that of previous global fits, such as CTEQ5HJ. A detailed study of the impact of these jet data on the determination of gluon distributions and the potential for observing signals for new physics at the Tevatron and the LHC will be carried out in a separate study.

3.1.2 The New Parton Distributions in the \overline{MS} scheme

Figure 7 shows an overview of the comparison between the new PDF's and the previous generation of CTEQ PDF's, the CTEQ5M1 set, at $Q = 2$ GeV. In order to exhibit the behavior of the PDF's clearly for both large and small x in one single plot, we choose the abscissa to be scaled according to $x^{1/3}$. Correspondingly, we multiply the ordinate by the factor $x^{5/3}$, so that the area under each curve is proportional to the momentum fraction carried by that flavor in the relevant x range. We see that the most noticeable change occurs in the gluon distribution.

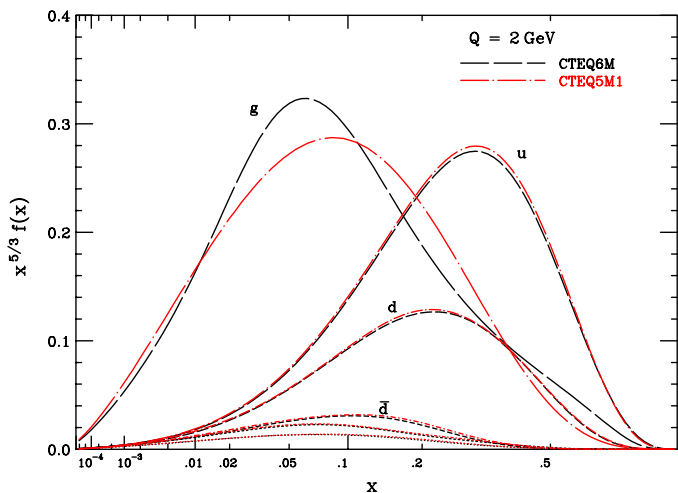


Figure 7: Comparison of CTEQ6M (dashed) to CTEQ5M1 (dot-dashed) PDF's at $Q = 2$ GeV. (The unlabeled curves are \bar{u} and $s = \bar{s}$.)

The gluon distribution Figure 8 gives a more detailed picture of the changes in the gluon distribution at $Q = 2$ and 100 GeV. For low and moderate values of x , say $10^{-5} < x < 0.1$, the most important constraint is due to the rate of Q^2 -evolution of the DIS structure functions. The HERA data in this region are ever improving in accuracy, but the new data has not made a sizable change in the gluon distribution, as seen in Figs. 7 and 8a. (Below $Q = 2$ GeV, one may find larger deviations between the new and old distributions, but extrapolation of PDF's into that low- Q region is well known to be unstable. We will return to this point in Sec. 5.2.)

In the moderate to high x range, $x > 0.01$, the inclusive jet data are now playing a very important role. The combined effects of the precision DIS and jet data have made a

full $N \times N$ covariance matrix V . Our method of correcting for systematic errors on the data points, which depends on writing V in a separable form in terms of the $K \times N$ coefficients $\{\beta_{ji}\}$, Eqs. (2.1) and (2.2), cannot be apply in this case.

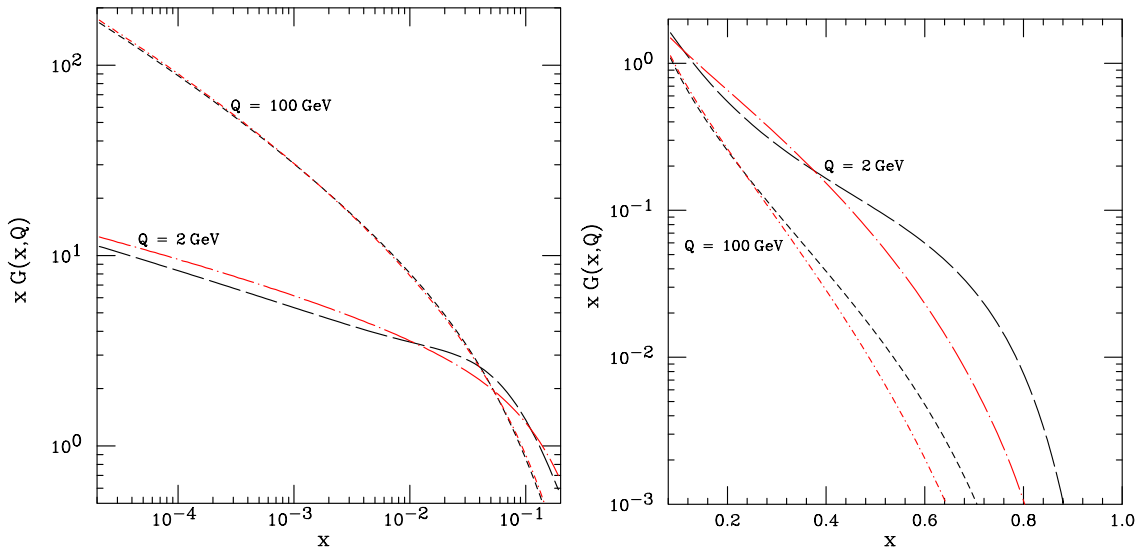


Figure 8: Comparison of CTEQ6M (dashed) to CTEQ5M1 (dot-dashed) gluon distributions at $Q = 2$ and 100 GeV. (a) The small- x region; (b) the large- x region.

significant shift in the shape of the gluon distribution, as seen in Figs. 7 and 8b. The new gluon distribution is significantly harder than for CTEQ5M1 and all MRST PDF sets (cf. Sec. 5.2) at all Q scales. This behavior is mainly dictated by the inclusive jet data, which lie in the range $50 < Q < 500$ GeV and $0.01 < x < 0.5$. The $D\bar{O}$ data in the higher η bins now allow a higher x reach than the central jet data from previous measurements. The hard gluon distribution becomes amplified at lower Q scales, due to the nature of QCD evolution and the fact that there is no direct experimental handle on the gluon at large x and low Q . The enhanced gluon at large x is similar to the CTEQ4HJ and CTEQ5HJ distributions. However, there is an important difference in the significance of the current result: whereas the “HJ” PDF sets were obtained specifically for fitting the high p_T jet data, by artificially inflating the weights of those points in the global fit, the CTEQ6M gluon distribution results naturally from the new global fit without any such special emphasis. The visually good fits seen in Figs. 5 and 6 are quantitatively substantiated by the small χ^2/N value of 118/123 for the jet data sets. Since CTEQ6M represents the “best fit” in the global analysis, this gluon behavior is also fully consistent with all DIS and Drell-Yan data sets used in the fit, as discussed previously.

3.1.3 DIS and LO Parton Distributions

For most applications, the \overline{MS} parton distributions are the most appropriate. But for certain applications, PDF’s in the NLO-DIS scheme are preferred. For these purposes we have obtained CTEQ6D by performing independent global fits in the NLO-DIS scheme. Although, in principle, one could obtain NLO-DIS parton distributions by a simple transformation from a NLO- \overline{MS} set, the reliability of such a procedure is uncertain in x regions where the numerical values of the PDF’s for different flavors (which transform into each

other) are orders of magnitude apart.⁸ It is thus preferable to perform an independent fit. The quality of fit for the NLO-DIS fit is comparable to that of the \overline{MS} case.

Leading-order (LO) parton distributions are most useful for Monte Carlo (MC) event generator applications, and also for simple estimates of high-energy cross sections. In performing leading-order fits, one uses tree-level formulas for the hard cross sections, and parton distribution functions evolved with leading-order splitting functions. For the $\alpha_s(Q)$ function, one can either use the LO formula for formal consistency, or use the NLO formula which is arguably more appropriate for MC applications in which many higher-order effects are included by the event-generator program. For this reason, we present two sets of LO fits: (i) CTEQ6L uses the same $\alpha_s(Q)$ function as the standard NLO fits (CTEQ6M, CTEQ6D, and the eigenvector sets) with $\alpha_s(M_Z) = 0.118$; and (ii) CTEQ6L1 uses the LO formula for $\alpha_s(Q)$ with $\Lambda_{QCD}^{(4flavor)} = 0.215$ GeV (which corresponds to $\alpha_s^{(1)}(M_Z) = 0.130$). When used with the corresponding (i.e., NLO or LO respectively) $\alpha_s(Q)$, both of these are good fits to the global data, within the uncertainty range of our analysis.

3.2 Eigenvector PDF Sets For Uncertainty Analyses

As mentioned in the Introduction and in Sec. 2.3, an important goal of this work is to advance global QCD analysis to include systematic and quantitative estimates of uncertainties—on both PDF’s and their physical predictions. For this purpose, we characterize the behavior of the global χ^2 function in the neighborhood of the minimum by a set of eigenvector PDF sets, according to the method of [11] (cf. the illustration in Sec. 2.3).

The eigenvector sets are obtained in two steps. First, the full set of parameters described in Sec. 2.5 is probed with the iterative procedure of [10, 11], in order to identify those parameters that are actually sensitive to the input data set.⁹ With current data, and our functional form, 20 such parameters are identified. We then generate the eigenvector PDF sets in the 20 dimensional parameter space as described in [10, 11], with the remaining parameters held fixed. This results in 40 PDF sets, a + (up) and a – (down) set for each eigenvector direction in the parameter space, in addition to the central CTEQ6M set. Ideally, in the quadratic approximation of the Hessian approach, the χ^2 curves would be symmetric around the minimum, so that only one displacement would be needed for each eigenvector. However, we observe some asymmetry in certain directions in practice, so we have decided to generate both up and down sets in each eigenvector direction; this provides more information on the behavior of constant- χ^2 surfaces in the neighborhood of the minimum.¹⁰ The up/down sets, called $S_1^+, S_1^-, \dots, S_{20}^+, S_{20}^-$, correspond to a *tolerance* of $T = 10$ (cf. Ref. [11]); i.e., their χ^2 value is greater than the minimum by $T^2 = 100$.

⁸A recently discovered [34] error in the QCD evolution of DIS scheme PDF’s in previous CTEQ analyses has been corrected in this work. This error has negligible practical consequences in physical applications in the current energy range, because the small deviation in evolution was naturally compensated by the fitted PDF’s. As long as the same DIS hard cross sections are used in the fitting and in the applications, as is indeed the case, the same physical cross sections will be reproduced. We thank G. Salam for useful communications on this issue.

⁹The sensitive parameters are those that are not close to “flat” directions in the overall parameter space, as mapped out by the iterative diagonalization procedure of [10].

¹⁰This asymmetry has been encountered in some applications, e.g. Ref.[35].

The range of uncertainty corresponding to the choice $T = 10$ represents our estimate of the range of PDF behavior that is consistent with the current data. Details of the error analysis that leads to this estimate are described in Appendix B.4.

3.2.1 Uncertainties of PDF's

We use the eigenvector PDF sets $\{S_i^\pm\}$ to estimate the uncertainty range of physical quantities (and of the PDF's themselves) according to the master equation (2.3) which is derived in [11]. In Figs. 9 and 10 we show fractional uncertainty bands for the u -quark, d -quark, and gluon distributions, respectively, at $Q^2 = 10 \text{ GeV}^2$. In these plots, the shaded region is the envelope of allowed variation of the parton distribution, independently for each value of x , with tolerance $T = 10$. The ordinate is the ratio of the extreme value (up or down) to the standard CTEQ6M value. For comparison, the curves are CTEQ5M1 (dashed) and MRST2001 (dotted), plotted in ratio to CTEQ6M.

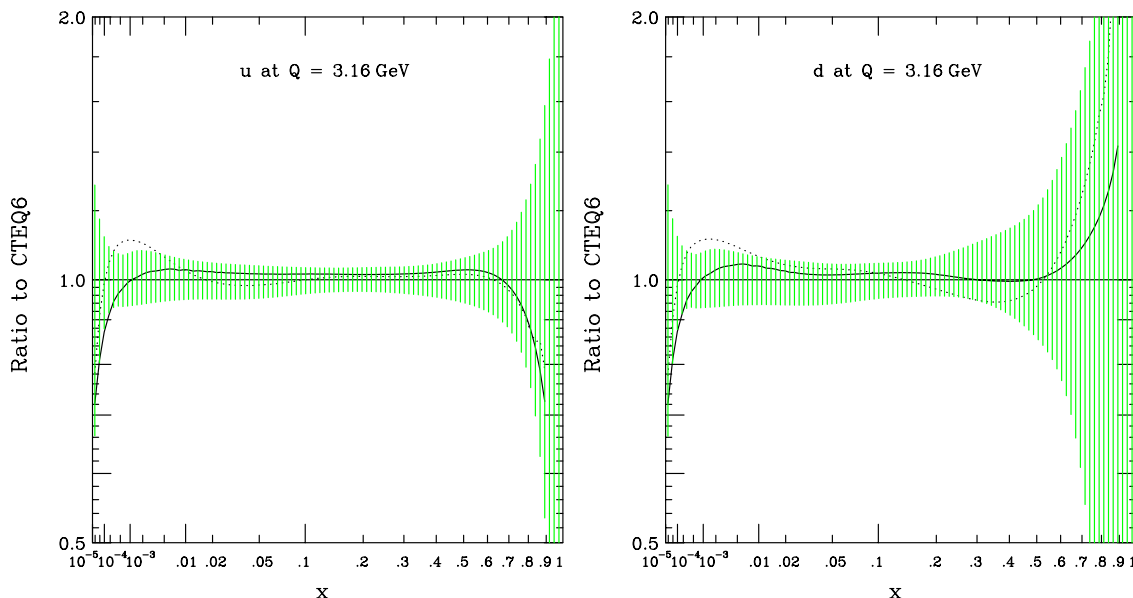


Figure 9: Uncertainty bands for the u - and d -quark distribution functions at $Q^2 = 10 \text{ GeV}^2$. The solid line is CTEQ5M1 and the dotted line is MRST2001.

The u distribution is the most accurately known of the parton distributions, since deep-inelastic scattering by photon exchange, being proportional to the square of the quark charge in leading order, is most sensitive to the u quark. The d -quark distribution is very much affected by the various data sets that are sensitive to u - d differences: the NC and CC DIS measurements with proton and deuteron targets, the DY p/d asymmetry and the W -lepton asymmetry experiments. The d -quark uncertainty band is seen to be noticeably wider than that of the u quark, particularly at large x where there are few constraints on the ratio between the two flavors. This result provides quantitative confirmation of a previous study [36], addressing the issue of the behavior of the d -quark distribution at large x raised in [37].

The gluon distribution is the most uncertain of the PDF's—notwithstanding the increased constraints from recent precision DIS and inclusive jet data discussed earlier—as shown in Fig. 10. The uncertainty is of order $\pm 15\%$ for x values up to ~ 0.3 , and then it increases rapidly for large x . This uncertainty is of much interest for the physics programs of the Tevatron and the LHC, and it has been the subject of several previous studies [38]. With the new quantitative tools at hand, we have found that it is important to use a sufficiently flexible parametrization of the initial distribution, in order to obtain a reliable estimate of the range of uncertainty of the gluon distribution. This point will be relevant when we compare the above result with other recent studies of the gluon distribution (cf. Sec. 5.2). Some details are given in Appendix D.

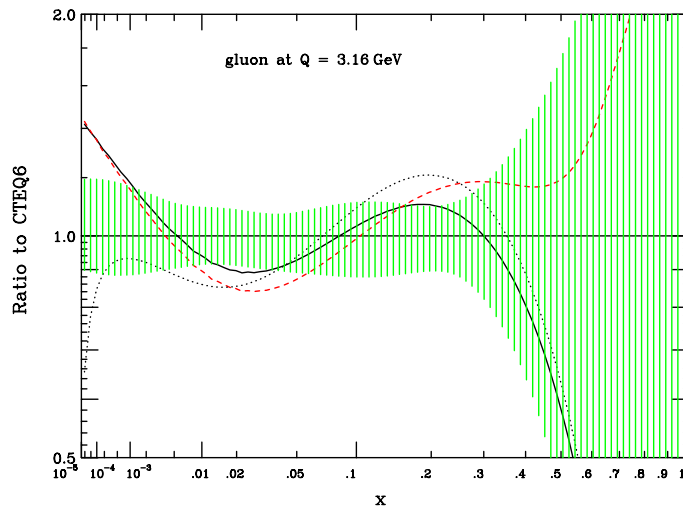


Figure 10: Uncertainty band for the gluon distribution function at $Q^2 = 10 \text{ GeV}^2$. The curves correspond to CTEQ5M1 (solid), CTEQ5HJ (dashed), and MRST2001 (dotted).

The uncertainties shown in Figs. 9 and 10 are significantly smaller than those obtained in our previous study [11] based on CTEQ5 inputs. The reduced uncertainty, which can be seen by comparing Figs. 9 and 10 with their counterparts (Figs. 3 and 4) of Ref. [11], is a consequence of the new DIS and jet data.¹¹

An important point in the interpretation of Figs. 9 and 10 is that the uncertainty ranges correspond to the envelopes of possible parton distributions that are consistent with the data. A distribution function that produces the extreme at any particular value of x is generally not extreme at other values of x . Thus, a PDF that follows the upper or lower boundary of the uncertainty band at all x would definitely not be consistent with the data.

The CTEQ5M1 and MRST2001 distributions, plotted as ratios to CTEQ6M, are also shown on Figs. 9 and 10, for comparison. Both these PDF sets are generally within the current uncertainty bounds. The hard gluon distribution in the CTEQ6M fit, discussed earlier, manifests itself in the fact that both CTEQ5M1 and MRST2001 curves are close to the lower limit of the uncertainty band at large x . For comparison, we have also included

¹¹One must be aware that the uncertainties shown in [11] are for a higher value of $Q = 10 \text{ GeV}$. The uncertainties decrease when evolved to higher Q .

the gluon distribution of CTEQ5HJ in Fig. 10. It is even harder than that of CTEQ6M at $x > 0.3$, but still within the uncertainty band. Comparisons of CTEQ6M and CTEQ5M1 fits are discussed in the next subsection (3.3.1). The MRST2001 distributions are rather similar to CTEQ5, except at very small x where the gluon is smaller and the quarks are larger, both slightly outside the uncertainty ranges. Differences between CTEQ6 and MRST2001 fits are discussed in some detail in Sec. 5.2.

3.3 Issues And Comments

3.3.1 How much progress has been made?

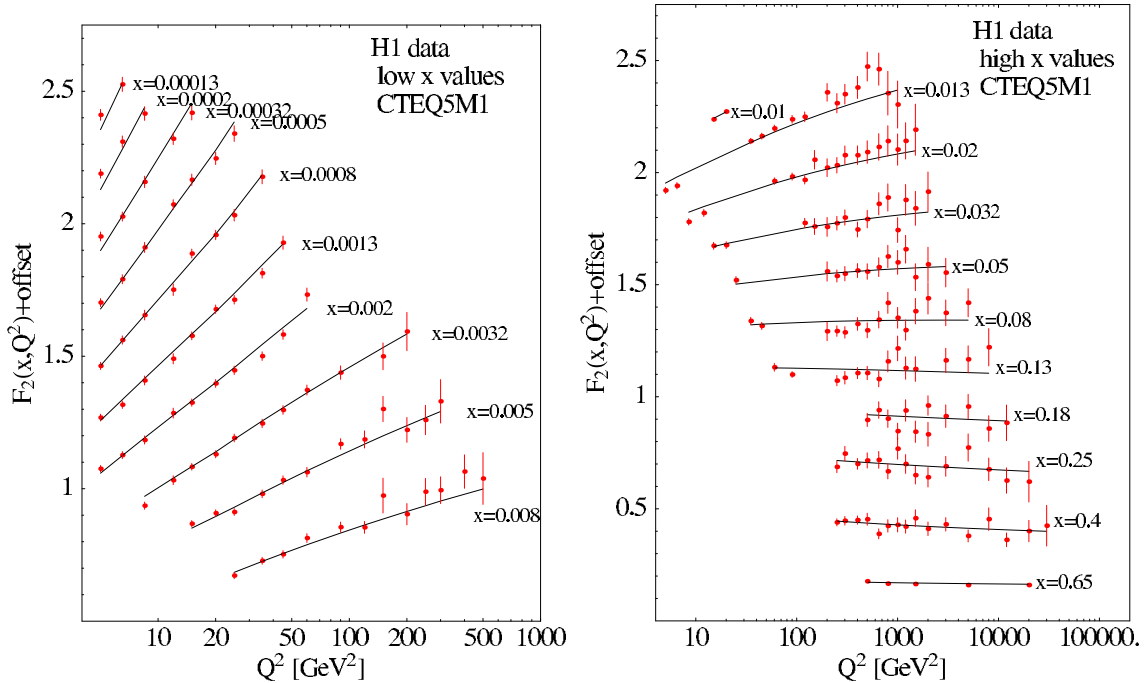


Figure 11: Comparison of the CTEQ5M1 predictions to the recent H1 data. Cf. format of Fig. 2.

The fact that the new PDF's, especially the quark distributions, do not appear to differ much from the CTEQ5 functions testifies to the steady convergence of QCD analysis of PDF's. Progress in this undertaking must be measured in more precise terms than previously, because of the increasing demands for quantitative applications in precision SM studies and new physics searches. To illustrate this point, we first compare the predictions of the preceding generation of PDF's, CTEQ5M1, with two key new experiments, H1 and DØ, in Figs. 11 and 12. Plots like these are often used in the literature as evidence of good or acceptable fits. Careful comparison with the corresponding results for CTEQ6M (Fig. 2 and Fig. 6) reveals that the new fit is discernably better.

The improvement in the quality of the fits can be quantified by examining the χ^2 values. With the inclusion of correlated systematic errors these numbers now carry more statistical significance than before. The accompanying table lists the CTEQ6M and CTEQ5M1 χ^2 's

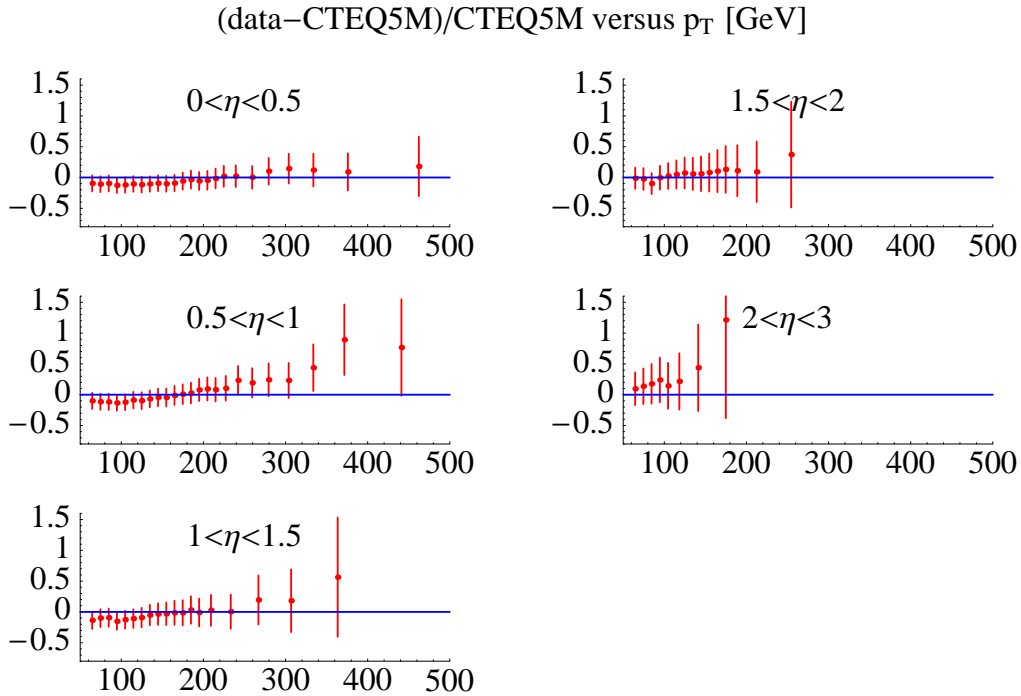


Figure 12: Comparison of the CTEQ5M1 predictions to the recent DØ data as in Fig. 5.

for the full data sets used in the current global analysis, and for the two representative experiments, H1 and DØ, shown in Figs. 11 and 12. The overall χ^2 is greater by 268 (for 1811 data points) for the previous generation of PDF's than the current one. The difference is not very large,¹² but it is outside our estimated tolerance of $T = 10$ ($\Delta\chi^2 = 100$).

The increases in the individual χ^2 's for the two precision experiments, although not very large, do lie outside the 90% probability range according to the uniform way we adopt for evaluating the uncertainty ranges, discussed in Appendix B.4. These numbers provide a quantitative measure of the improvement achieved. The precise interpretation of these numbers is still open to discussion, however, and further progress is still needed (cf. Appendix B.4).

χ^2 (# data pts.)	Total (1811)	H1 (230)	DØ (90)
CTEQ6M	1954	228	69
CTEQ5M1	2222	285	110

3.3.2 Higher twist terms?

There have been several studies of higher-twist (HT) effects in DIS experiments [5, 39, 40]. If power-law corrections to leading-twist PQCD are needed, they will introduce additional nonperturbative degrees of freedom in the global analysis. This would complicate PDF

¹²In evaluating these χ^2 numbers for the two fits, the overall normalizations of all the data sets are allowed to re-adjust, within errors, between the two calculations. Otherwise, the difference in χ^2 would be larger.

analysis considerably, because the extracted PDF's would then depend on the HT model. Because there is no accepted theory of HT, and HT terms are probably non-factorizable and process-dependent, PDF's obtained with the inclusion of HT terms would no longer be universal.

In the absence of firm theoretical guidance, we first limit the possible size of higher-twist terms by placing reasonable cuts on the kinematic range of data utilized in the fitting program. We then study phenomenologically the need for HT corrections by comparing the quality of fits with and without HT parameters. Using the same kinematic cuts as in previous CTEQ analyses (in particular, $Q \geq 2 \text{ GeV}$ and $W \geq 3.5 \text{ GeV}$ for DIS data) we find that the inclusion of simple phenomenological HT factors, of the type used in the previous literature [5, 39, 40], does not produce discernable improvement in the quality of the fit. We conclude that HT corrections are not needed, and therefore stay within the twist-2 PQCD formalism for our analysis.¹³ Our study of this issue is summarized in Appendix C. We believe, for the reasons mentioned in the previous paragraph, that should there be evidence for HT effects, it would be more desirable to raise the kinematic cuts and preserve the universal PDF's, rather than to introduce *ad hoc* HT terms that would reduce the usefulness of the PDF's.

3.3.3 Signs of anomalies at large x or small x ?

One of the important goals of quantitative global analysis of PDF's is to provide stringent tests of the validity, and the efficacy, of PQCD. Anomalies observed in one or more of the hard processes in the global analysis could indicate signs of new physics.

Among the hard processes in current global analyses, the high- E_T jet cross section measured by CDF and DØ probes the smallest distance scales, and hence provides the best window to discover new physics at large energy scales. There was some excitement when CDF first measured a possible excess in the high- E_T jet cross section, compared to conventional PDF predictions of that time [41]. This excitement has abated with the advent of the “PDF explanation” [42] (the CTEQ4HJ and CTEQ5HJ type of gluon distributions [2]) and the subsequent DØ measurements [43] (which do not show as pronounced an effect). However, the issue remains an interesting one since the CTEQ4HJ/5HJ gluon distributions have not been universally accepted as the PDF of choice. Where does the issue stand in view of the recent data and global analyses?

As already mentioned in Sec. 3.1.2 above, the CTEQ6M central fit arrives at a gluon distribution that is considerably harder at high x than the conventional ones (such as CTEQ5M and MRST2001). It is more like CTEQ4HJ and CTEQ5HJ, although obtained without giving any extra weight to the jet data. This change comes about from three developments: (i) the statistical power and the expanded range of the new DØ jet data set in the five separate rapidity intervals [16]; (ii) the increased flexibility of the nonperturbative gluon distribution in the new parametrization adopted for this global analysis (cf. Secs. 2.5,

¹³This conclusion may appear to contradict some common lore about HT. We note that most of the previous studies either were not done with as wide a range of data sets, or did not incorporate the full correlated systematic errors. Also, we use a relatively high Q^2 cut of 4 GeV^2 , precisely to reduce the HT effects.

5.2 and Appendix D); (iii) the fact that the harder gluon is needed to provide a better fit to the $D\bar{O}$ data. On one hand, this result provides further support for the PDF explanation of the high- E_T jet cross section. On the other hand, by the more quantitative uncertainty analysis shown in Fig. 10, there is still a large range of possible behavior for the high- x gluon, allowing both the conventional and the ‘‘HJ-like’’ shapes. Further work will be required to draw a firm conclusion on this important issue. Continued search for signs of new physics must be pursued with vigor in all channels.

Signals for a departure from conventional PQCD could also appear in the very small x region. Our analysis is based on the standard NLO DGLAP formalism. The impressive agreement between the fits and all the data sets shows no indication of a breakdown of conventional PQCD; nor do we detect any necessity for including NNLO corrections [44]. This does not mean that effects beyond the simple theoretical model are not present. It does mean that the search for these effects must depend on even more precise, and extensive, experimental and theoretical input.

3.3.4 Determination of α_s ?

As mentioned in Sec. 2.5, for our standard analysis we input the strong-coupling strength $\alpha_s(m_Z) = 0.118$, based on dedicated measurements from QCD studies at e^+e^- colliders and sum rules in lepton-hadron processes. It is desirable to check that this value is consistent with our global analysis, and, beyond that, to see whether the global analysis can provide a useful independent measurement of α_s .

For this purpose, we have repeated the fitting with different choices of $\alpha_s(m_Z)$. The resulting variation of the global χ^2 is shown in Fig. 13. The minimum in χ^2 occurs at a value of $\alpha_s(m_Z) \simeq 0.1165$, somewhat lower than the world average from precision measurements. For our choice of $\alpha_s(m_Z) = 0.118$, χ^2 is greater than the minimum by about 5. This difference is completely insignificant with respect to our estimated tolerance of $\Delta\chi^2 < T^2 \approx 100$. Thus, the value of $\alpha_s(m_Z)$ favored by global PDF analysis is in excellent agreement with the world average. Furthermore, according to Fig. 13 and our adopted tolerance, the allowed range of $\alpha_s(m_Z)$, as measured in global PDF analysis, is about 0.110 to 0.123 (i.e. $\alpha_s(m_Z) = 0.1165 \pm 0.0065$). This is not competitive with other dedicated measurements. The basic reason is well known: the uncertainty of α_s determination in QCD analysis of parton distributions is strongly tied to the uncertainty of the gluon distribution, which still has substantial uncertainties.

We also note that the definition of NLO $\alpha_s(\mu)$ in perturbative QCD is subject to an ambiguity relating to the solution of the renormalization group equation (RGE). We have used the conventional \overline{MS} formula for $\alpha_s(\mu)$, obtained by solving the NLO RGE as an expansion in inverse powers of $\ln \mu$ [28]. An alternative definition, favored by some, and more convenient for higher-order extensions, is to numerically solve the truncated RGE equation for $\mu d\alpha/d\mu$ at NLO. The dotted curve in Fig. 13 shows χ^2 versus $\alpha_s(m_Z)$ using this alternative definition of $\alpha_s(\mu)$. The difference between the two treatments is seen to be within the range of uncertainties.

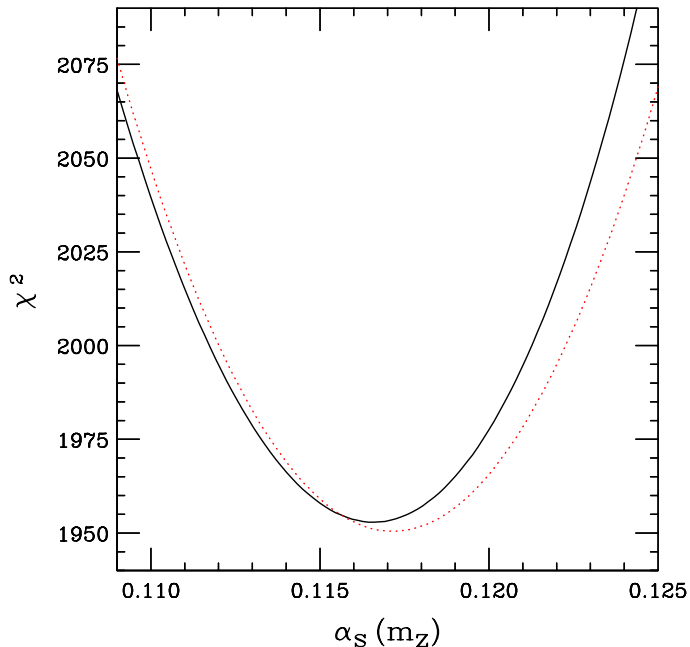


Figure 13: χ^2 vs. $\alpha_s(m_Z)$ curve, with two alternative definitions of the NLO α_s .

3.4 User Interface

All PDF sets described above will be available (at <http://cteq.org>) in the usual CTEQ format, using external data tables. These can be used in the same way as previous CTEQ PDF's.

In addition, to facilitate progress toward a universal user interface, we are preparing a new format, which uses an evolution program and small external files containing only the coefficients for the initial parton distributions, following the “Les Houches Accord on PDF's” [45].

4. Physical Predictions and their Uncertainties

The main utility of the new parton distribution functions is to make predictions on physical cross sections and their uncertainty ranges—both for precision SM studies and for new physics searches. Detailed applications go beyond the scope of this paper. We will, however, present some general results on estimated uncertainties of various parton luminosity functions for the Tevatron (RunII) and the LHC. From these results, one can easily estimate the expected uncertainties of a variety of physical processes of interest for these hadron collider programs: W/Z cross sections, Higgs, and top (both single and pair production) rates due to various production mechanisms, etc.

Figure 14a shows the fractional uncertainties of the gluon-gluon and quark-antiquark luminosity functions, to final states with the quantum numbers of W^\pm , W^- , γ^* and Z^0 , at the Tevatron. Figure 14b similarly displays the quark-gluon luminosity functions for W^+ , W^- , γ^* , Z final-state quantum numbers. As expected, the gluon-gluon luminosity has

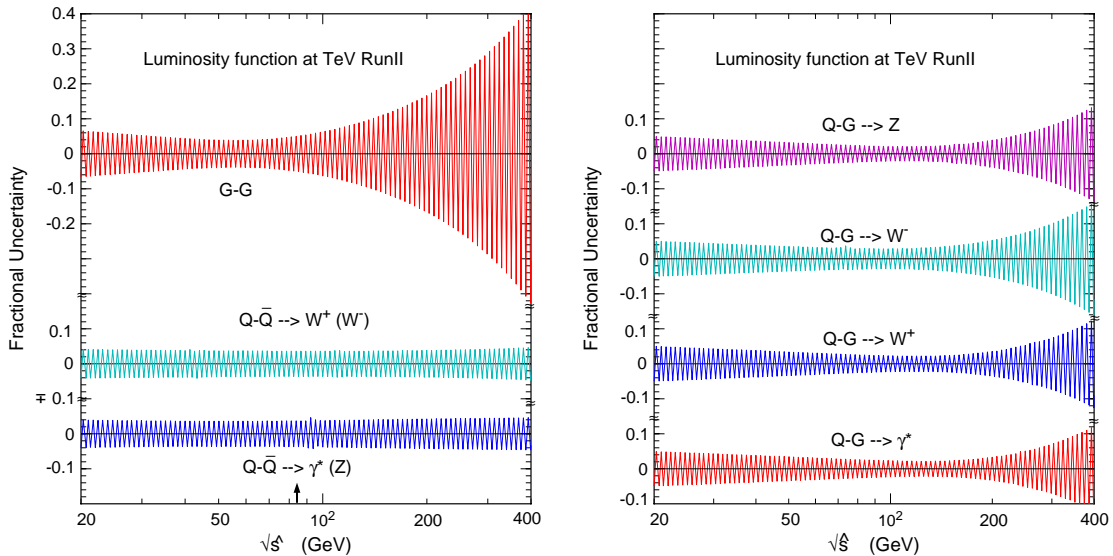


Figure 14: Uncertainties of the luminosity functions at the Tevatron.

the greatest uncertainty, especially at large $\sqrt{\hat{s}}$, reflecting the uncertainty of the gluon distribution at large x . The $q\bar{q} \rightarrow W^+, W^-, \gamma^*, Z$ luminosity uncertainties are almost constant throughout the range of $\sqrt{\hat{s}}$ plotted, at the $\pm 4\%$ level. The $qG \rightarrow W^+, W^-, \gamma^*, Z$ luminosity uncertainties resemble the geometric mean between those for GG and qG . The four qG uncertainty bands are very similar to one another, but close examination shows that they are not identical, because of the differences in quark flavor mix.

Similarly, Fig. 15 shows the fractional uncertainties of the corresponding luminosity functions for the LHC. The $q\bar{q} \rightarrow W^\pm$ luminosity uncertainties are also fairly constant, being $\pm 5\%$ for $q\bar{q} \rightarrow W^+$ and $\pm 4\%$ for $q\bar{q} \rightarrow W^-$ for $100 < \sqrt{\hat{s}} < 200 \text{ GeV}$. The gluon-gluon luminosity uncertainty is $\pm 3\%$ at the narrowest point ($\sqrt{\hat{s}} \sim 250 \text{ GeV}$), increasing to $\pm 10\%$ at both ends of the $\sqrt{\hat{s}}$ range shown. From this, one can estimate that the uncertainty on the production cross section of a light mass Higgs particle (say, 100–200 GeV) at the LHC due to PDF's is on the order of $\pm 5\%$. The uncertainty of the gluon-gluon luminosity function at the LHC is seen to be generally smaller than for the Tevatron case. The difference results from the combination of two effects: the uncertainty decreases with evolution, and the contributing x ranges for the two cases are somewhat different. The luminosity uncertainties for the Compton processes at the LHC, Fig. 15b, are again rather similar to one another. The uncertainties range from around $\pm 6\%$ at low energies to $\pm 2 - 3\%$ at $\sqrt{\hat{s}} \sim 500 \text{ GeV}$.

The W cross section can be measured with great precision at hadron-hadron colliders. The cross section is large and the backgrounds are relatively small. In addition, the theoretical uncertainties are small. This makes the W cross section an ideal benchmark with which to normalize other cross sections, especially as there remains a significant uncertainty as to the value of the total inelastic cross section at the Tevatron. (The inelastic cross section is

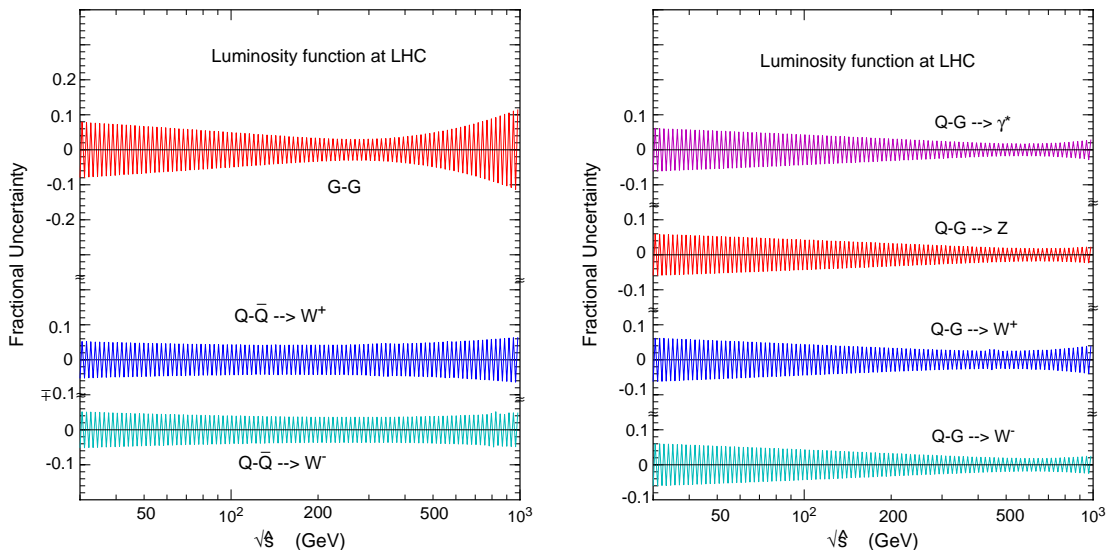


Figure 15: Uncertainties of the luminosity functions at the LHC.

used by the experimental collaborations to normalize all luminosity calculations. CDF and DØ currently assume values for this cross section that differ by 6%, producing cross-section differences between the two experiments of the same amount.) The simple estimates of the W cross section uncertainty the PDF uncertainties at the Tevatron and the LHC, given above, can be improved by including NLO terms and by using the more precise Lagrange method [12]. Using the 40 Hessian eigenvector sets, the uncertainty for any cross section can be calculated. This procedure will be made more straightforward with the adoption of the Les Houches accord on PDF's.

5. Comparison with Other Parton Distribution Analyses

5.1 Previous Uncertainty Studies

The quantitative analysis of uncertainties of PDF's, taking into account the experimental systematic errors, was pioneered by [4–6], in the context of detailed study of the precision DIS experiments. These studies were based on χ^2 minimization techniques. The methods that we developed in [10–12], and used in this paper, have extended this approach to a global analysis (cf. the recent review [26].) Because the scope of the experimental data used in the earlier studies is different from ours, direct comparison with those results is not possible.

Giele et al. (GKK) advocate a more general approach, using a pure probabilistic analysis with random sampling of the parton parameter space [7]. While theoretically appealing, the proposed method encounters difficulties when confronted with real experimental data sets, which either do not meet the strict statistical criteria or are mutually incompatible according to a rigorous probabilistic interpretation of the errors. As a result, although the

methodology is clearly established, it has not yet produced practical results that can be generally used.

In an ideal world, where all experimental data sets are self-consistent and mutually compatible, the GKK method is equivalent to the one we use, provided, in addition, the Gaussian approximation underlying the χ^2 approach is valid. If, however, χ^2 is not approximately quadratic in the neighborhood of the minimum, and if the precise response functions for all experiments in the global analysis are known, then the GKK method would be superior. Minimization of χ^2 could still be useful in that case, but the accuracy is only as good as the Gaussian approximation. In reality, of course, the detailed experimental response functions are rarely, if ever, known. So realistically the study of PDF uncertainty will necessarily consist of quantitative statistical analysis supplemented by pragmatic choices based on physics considerations and experience.

5.2 Comparison to MRST2001

Our results can be compared more directly to those of the recent MRST2001 analysis [13]. An overview of the comparison between the CTEQ6M and MRST2001 parton distributions is shown in Figure 16. Significant differences appear in the gluon distribution, similar to the differences between CTEQ6 and CTEQ5 described in Sec. 3.1.2. Unlike CTEQ5, the MRST analysis uses essentially the same recent experimental input as CTEQ6. Thus it is natural to seek the sources of the observed differences.

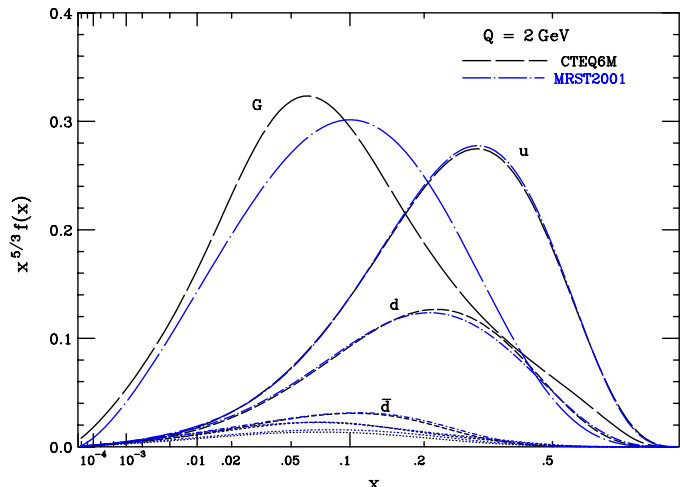


Figure 16: CTEQ6M PDF's compared to MRST2001. (The unlabeled curves are \bar{u} and $s = \bar{s}$.)

Although most of the experiments used in the CTEQ6 and MRST2001 analyses are the same, there are some differences both in data sets and in the way that experimental error information is utilized. The CTEQ6 analysis uses the separate-energy data sets of the BCDMS and NMC experiments (for which information on correlated systematic errors is available) whereas MRST uses the combined-energy sets for these experiments. The CTEQ6 analysis does not use SLAC experiments, because that data lies in the region of very low Q^2 . Also, CTEQ6 does not use the HERA charm-production data, because the

errors are still large, and because a proper theoretical treatment of this process requires the full inclusion of charm mass effects in the matrix elements.¹⁴ In addition, the kinematic cuts on data selection are somewhat different.

There are several differences in methodology. In the analysis of data, the published experimental correlated systematic errors are fully incorporated in the CTEQ6 global fitting procedure. In the theoretical calculations, we use the conventional (zero-mass parton) Wilson coefficients for DIS structure functions for reasons explained in Sec. 2.4, whereas MRST uses the Thorne-Roberts version of the VFNS calculation [30]. Finally, the two groups use different functional forms for the parametrization of the nonperturbative input parton distributions.

Beyond a visual inspection of the PDF's, insight can be gained by comparing the two fits for data sets used in both analyses. In principle, one might just compare the χ^2 values of the corresponding experiments for the two fits, cf. χ^2 numbers given in Appendix A and Table 1 of Ref. [13]. In practice, a direct comparison between the DIS experiments is not possible because the two analyses have different treatments of the experimental systematic errors and different choices of Wilson coefficients mentioned above. Among experiments that can be directly compared, two differences are noticeable. The first experiment is E605 (Drell-Yan): χ^2/N is given as 232/136 in MRST2001 [13], and 95/119 for CTEQ6M.¹⁵ However, the seemingly large MRST number was due to their use of statistical errors only for this experiment. The two fits are actually comparable for this experiment. The second is the combined DØ and CDF jet cross section measurements: χ^2/N is 170/113 for MRST2001, and 118/123 for CTEQ6M. This difference is statistically quite significant, and it is responsible for the rather distinct gluon distributions obtained by the two groups. We believe that this difference is primarily due to the parametrization of the nonperturbative parton distributions, especially the gluon, as will be discussed below and in Appendix D.

We now comment more specifically on a number of issues highlighted in the MRST paper [13] from the perspective of the current study.

Large- x gluon behavior The inclusive jet data have a strong influence in the determination of the gluon distribution at medium and large x . The MRST analysis found a rather significant competition between the jet data and the Drell-Yan (E605) data in the context of their global fit. This requires either a compromise, the MSRT2001 set, or a good fit to the jet data with a much poorer Drell-Yan fit (and a rather unusual gluon shape), the MRST2001J set [13].

This dilemma is not observed in our analysis. The CTEQ6M fit to both the jet data and the Drell-Yan data appear nearly “ideal” (i.e., $\chi^2/N \sim 1$), and the gluon shape is rather smooth. This clear difference results mainly from the parametrization of the PDF's, especially that of the gluon. We are led to this conclusion by a study where we adopt the MRST parametrization for the gluon and repeat the global fit. We then obtain a “best fit” in which the gluon has a shape similar to MRST2001J. The gluon distributions at

¹⁴Work is under way for inclusion of charm production in a separate global analysis.

¹⁵The differences in the number of data points are due to slightly different kinematic cuts in the two analyses.

$Q = 2$ GeV for CTEQ6M, MRST2001, MRST2001J, and the MRST-like fit that we obtain by adopting the MRST parametrization are compared in Figure 17. The “wobble” of the gluon function observed in the latter two fits (which led MRST to reject the MRST2001J fit [13]) is clearly due to the particular functional form. More details, including other examples and results at $Q = 1$ GeV (which are more sensitive to the differences), are presented in Appendix D on the question of parametrization.

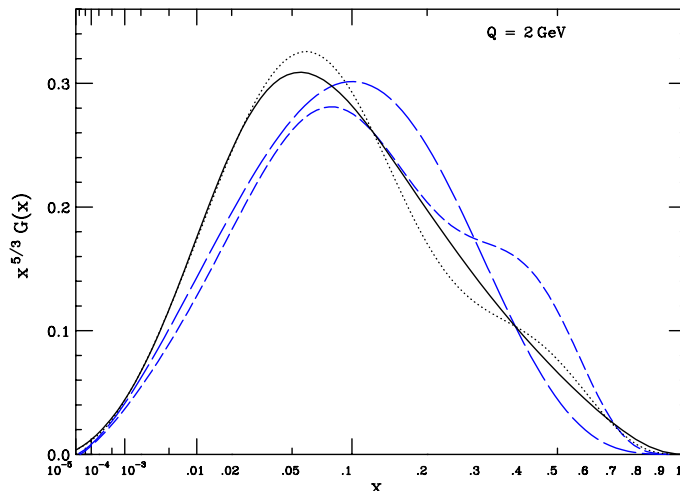


Figure 17: Comparison of the gluon distributions at $Q = 2$ GeV, for CTEQ6M (solid), MRST2001 (long-dashed), MRST2001J (short-dashed) and the MRST-like fit (dotted).

Gluon behavior at small x and small Q The MRST study found a strong preference for a negative gluon distribution at small x and small Q . It has been known for a long time that QCD evolution is extremely rapid at small Q . This makes extrapolation *backward* to $Q = 1$ GeV quite unstable [46], even though the behavior of the PDF’s at $Q > 2$ GeV is rather tightly constrained by the experimental data. It is generally agreed that there is no theoretical requirement that parton distributions be positive definite at any particular Q , as long as cross section predictions stay positive. The issue is, thus, only a phenomenological one.

We have chosen $Q_0 = 1.3$ GeV for the CTEQ6 fit, and find no indication for $G(x, Q)$ going negative in the region $Q > 1.3$ GeV. To consider lower values of Q , we have made alternative fits with Q_0 down to 1.0 GeV which are described in Appendix D. The results can be summarized as follows: (i) Whether or not the gluon distribution tends to go negative is strongly dependent on the choice of Q_0 —it will always go negative at some low Q , as anticipated in [46]. (ii) With $Q_0 = 1$ GeV, parametrizations that allow for a negative gluon at small x can yield slightly lower χ^2 than those with positive-definite gluons. This has no phenomenological significance, however, since the difference between the resulting gluon distributions is much smaller than its uncertainty in this region. The uncertainty assessment is closely related to the study of parametrization described in Appendix D. Note, in particular, Fig. 24b.

Measurement of α_s MRST performed an analysis to determine $\alpha_s(m_Z)$ from their global fits, obtaining $\alpha_S(m_Z) = 0.119 \pm 0.002$ (expt.) ± 0.003 (theory). As discussed in Sec. 3.3.4, our study obtained a lower central value and a substantially larger error estimate. The latter (± 0.002 vs. ± 0.0065) is mainly due to the different choices of allowed $\Delta\chi_{\text{tot}}^2$ (20 vs. 100). In fact, in order to achieve $\Delta\alpha_S(m_Z) = \pm 0.002$ (expt.) from Fig. 13, we would have to use $\Delta\chi_{\text{tot}}^2 \sim 10$. In view of our study of the overall tolerance parameter discussed in Sec. B.4, we cannot justify having such a narrow range for $\alpha_s(m_Z)$, since many perfectly acceptable global fits exist within the full range $\alpha_S(m_Z) = 0.1165 \pm 0.0065$, even without including theoretical uncertainties.

6. Concluding Remarks

In this paper, a new generation of parton distribution functions has been presented, making full use of the constraints of both the old and new data. This global analysis significantly expands the scope of the currently used PDF analyses on two fronts: (i) a full treatment of available experimental correlated systematic errors, and (ii) a systematic treatment of uncertainties of the parton distributions and their physical predictions, using a recently developed eigenvector-basis approach to the Hessian method. Thus, in addition to obtaining new best-fit PDF's, the ranges of uncertainties of the PDF's and their physical predictions are systematically assessed.

Among the improvements made in PDF determination, progress on the gluon distribution is particularly worth noting. The new $D\bar{O}$ jet data play a significant role in obtaining a hard gluon distribution at large x —quite different from previous standard fits. We have shown that, at $Q^2 = 10 \text{ GeV}^2$, its uncertainty has been narrowed by recent precision data to $\pm 10\%$ at small x (up to $x \simeq 0.3$). The uncertainty then increases quite rapidly (in spite of the improved constraints), reaching a factor of 2 by $x \sim 0.5$. The need for additional precise data to pin down the gluon distribution over a larger x range is obvious. The excellent agreement between the new $D\bar{O}$ non-central jet cross sections and the precision DIS and DY data sets, within the PQCD framework using the new CTEQ6 PDF's, is significant. It lends credence to the PDF explanation of the earlier CDF high p_T jet measurement. A crucial element in achieving this consistent picture is to allow sufficient flexibility in parametrizing the nonperturbative parton distributions, in order to accommodate a range of possible behaviors at both low and high x .

The eigenvector basis PDF's obtained by this analysis allow the calculation of the uncertainty of any physical quantity that depends on the PDF's. We have presented results on parton-parton luminosity function uncertainties for both the Tevatron and the LHC. From these, uncertainties of a wide range of SM and new physics signals and backgrounds can be inferred. For instance, the uncertainties on the production cross sections of W, Z at the Tevatron and the LHC are estimated to be $\pm 4\%$ and $\pm 5\%$ respectively, and that of a light Higgs at the LHC to be $\pm 5\%$. More detailed calculations on the predicted cross sections and their uncertainties for processes of interest can easily be done, using the standard CTEQ6M and its associated eigenvector basis PDF's, or using the Lagrange method described in Ref. [12].

This work marks only the first step in the effort to advance the global analysis of PDF's, incorporating the systematic treatment of uncertainties. Improvements and applications of the results discussed in this paper are worth pursuing. It is also important to advance the theoretical input to the global analysis, including resummation effects, improved treatment of heavy quarks, and higher-order corrections. The current analysis is carried out at NLO and achieves a satisfactory fit to all of the data sets over a wide kinematic range. In the future, an extension to NNLO will be possible but this must wait until more cross-section calculations are available at the higher order, and until the precision of the experimental measurements makes it useful. In the near future, new data from both the Tevatron and HERA, along with further theoretical development, will allow for even more precise determinations of PDF's, leading to more useful predictions for LHC physics.

Acknowledgements We are pleased to acknowledge fruitful discussions and collaborations with many CTEQ colleagues over the years. Valuable suggestions on improvements to this manuscript have been provided by F. Olness, J. Owens, and D. Soper. J.P. and J.H. would like to thank many participants of the 2001 Les Houches Workshop, particularly S. Alekhin, M. Botje, W. Giele, and A. Vogt, for very active interaction on general issues relating to global QCD analysis of parton distributions. WKT acknowledges several stimulating discussions with M. Botje, W. Giele, and F. Zomer on the same topics.

The research of the authors is supported by the US Department of Energy, the National Science Foundation, the Lightner-Sams foundation, and the Taiwan National Science Council.

A. Details of the CTEQ6M fit

The coefficients for the nonperturbative PDF's at $Q_0 = 1.3 \text{ GeV}$, as defined in Sec. 2.5, for the CTEQ6M fit are:

	A_0	A_1	A_2	A_3	A_4	A_5
d_v	1.4473	0.6160	4.9670	-0.8408	0.4031	3.0000
u_v	1.7199	0.5526	2.9009	-2.3502	1.6123	1.5917
g	30.4571	0.5100	2.3823	4.3945	2.3550	-3.0000
$\bar{u} + \bar{d}$	0.0616	-0.2990	7.7170	-0.5283	4.7539	0.6137
$s = \bar{s}$	0.0123	-0.2990	7.7170	-0.5283	4.7539	0.6137
\bar{d}/\bar{u}	33657.8	4.2767	14.8586	17.0000	8.6408	-

The best fit to data is obtained with the following normalization factors for the experiments:¹⁶

Expt.(e)	BCDMS	H1a	H1b	ZEUS	NMC	CCFR	E605	DØ	CDF
Norm(e)	0.976	1.010	0.988	0.997	1.011	1.020	0.950	0.974	1.004

Table 1 shows the χ^2 values for those experimental data sets for which detailed information on systematic errors is available and used in the CTEQ6M fit. For each data set (e), we show: the number of data points (N_e), the χ^2 value for that experiment in the CTEQ6M fit (χ_e^2), and χ_e^2/N_e . These results form the basis for much of the quantitative uncertainty analysis discussed in this paper. The interpretation of the ZEUS and NMC χ^2 's are studied in some detail in Sec. B.3.¹⁷

Data sets with only effective uncorrelated errors are CCFR,¹⁸ E605, E866, and CDF W-lepton asymmetry. The nominal χ_e^2 / N_e for these data sets for the CTEQ6M fit are (150/156, 95/119, 6/15, 10/11) respectively.

data set	N_e	χ_e^2	χ_e^2/N_e
BCDMS p	339	377.6	1.114
BCDMS d	251	279.7	1.114
H1a	104	98.59	0.948
H1b	126	129.1	1.024
ZEUS	229	262.6	1.147
NMC F2p	201	304.9	1.517
NMC F2d/p	123	111.8	0.909
DØ jet	90	68.94	0.766
CDF jet	33	48.57	1.472

Table 1: Comparison of the CTEQ6M fit to data with correlated systematic errors.

B. Comparison of Theory and Data with Correlated Errors

This Appendix consists of (i) a brief summary of the formalism used in our error analysis—both for the χ^2 calculations in performing the global fits and for the interpretation of the results of those fits; (ii) an examination of the significance of the observed higher-than-nominal χ^2 's for two of the DIS experiments; (iii) a discussion of the estimated tolerance for our uncertainty estimates. Further details of the formalism can be found in Ref. [12].

¹⁶H1a and H1b refer to H1 data sets for low- Q and high- Q measurements respectively [14].

¹⁷The fairly large value of χ_e^2/N_e for the CDF data has been studied extensively by the experimental group [25]. A substantial part of the excess χ^2 is due to fluctuations of a few points at moderate p_T . The best value of χ_e^2/N_e that can be achieved for this data set (using a high order polynomial curve fit to the data) is approximately 1.3.

¹⁸See footnote 6, Sec. 3.1.1.

B.1 Useful formulas for χ^2 and the analysis of systematic errors

The simplest χ^2 function, used in most conventional PDF analyses, is

$$\chi_0^2 = \sum_{\text{expt.}} \sum_{i=1}^{N_e} \frac{(D_i - T_i)^2}{\sigma_i'^2} \quad (\text{B.1})$$

where D_i is a data value, T_i is the corresponding theory value (which depends on the PDF model parameters $\{a\}$), and σ_i' is the combined statistical and systematic errors (assumed uncorrelated and usually added in quadrature) on the measurement D_i . This effective χ^2 function provides a simple measure of goodness-of-fit, convenient for the search for candidate PDF sets by minimization. However, it is not useful for estimating the uncertainties associated with those candidates because it does not contain enough information to allow a meaningful statistical inference based on the increase in χ^2 away from the minimum.

Most DIS experiments now provide more detailed information on measurement errors. For each data point i , we have the statistical error σ_i , uncorrelated systematic error u_i , and several (say, K) sources of correlated systematic errors $\{\beta_{1i}, \beta_{2i}, \dots, \beta_{Ki}\}$. The best fit to the data (i.e., the fit with least variance) comes from minimizing the χ^2 function,¹⁹

$$\chi'^2(\{a\}, \{r\}) = \sum_{\text{expt.}} \left[\sum_{i=1}^{N_e} \frac{1}{\alpha_i'^2} \left(D_i - T_i - \sum_{k=1}^K r_k \beta_{ki} \right)^2 + \sum_{k=1}^K r_k^2 \right] \quad (\text{B.2})$$

where $\alpha_i'^2 = \sigma_i^2 + u_i^2$ is the combined uncorrelated error. The fitting parameters are (i) the PDF model parameters $\{a\}$, on which T_i depends, together with (ii) random parameters $\{r\}$ associated with the sources of correlated systematic error. The point of Eq. (B.2) is that D_i has a fluctuation $\sum_k r_k \beta_{ki}$ due to systematics. The best estimate of this shift is obtained by minimizing χ'^2 with respect to the set $\{r_k\}$. In practice, the total number of such parameters for all experiments included in the global analysis can be quite large. Adding these to the already large number of PDF parameters $\{a\}$ (which represent the real goal of the analysis) one encounters a formidable minimization task, involving a parameter space of dimension close to 100. The practical difficulties have considerably hindered past efforts using this approach. The stability and reliability of results obtained this way can also be questioned.

We pointed out in Ref. [12] that the minimization of the function χ^2 with respect to $\{r\}$ can be carried out analytically. This simplifies the global analysis to its irreducible task of minimization with respect to the PDF parameters $\{a\}$ only. In addition, the analytic method provides explicit formulas for the optimal values of $\{r_k, k = 1 \dots K\}$ due to the systematic errors $k = 1 \dots K$ that are associated with the fit. These optimal shifts are obtained from the condition $\partial\chi^2/\partial r_k = 0$, and the result is

$$r_k(\{a\}) = \sum_{k'=1}^K (A^{-1})_{kk'} B_{k'} \quad (\text{B.3})$$

¹⁹The prime is to distinguish it from the its simplified—but equivalent—form, χ^2 , derived below in Eq. B.5.

Here $\{B_k\}$ and $\{A_{kk'}\}$ are given by

$$B_k(\{a\}) = \sum_{i=1}^{N_e} \frac{\beta_{ki}(D_i - T_i)}{\alpha_i^2} \quad \text{and} \quad A_{kk'} = \delta_{kk'} + \sum_{i=1}^{N_e} \frac{\beta_{ki}\beta_{k'i}}{\alpha_i^2}. \quad (\text{B.4})$$

Substituting the best estimates (B.3) back into χ'^2 , we obtain a simplified χ^2 function,

$$\chi^2(\{a\}) \equiv \chi'^2(\{a\}, \{r(\{a\})\}) = \sum_{\text{expt.}} \left\{ \sum_{i=1}^{N_e} \frac{(D_i - T_i)^2}{\alpha_i^2} - \sum_{k,k'=1}^K B_k (A^{-1})_{kk'} B_{k'} \right\}. \quad (\text{B.5})$$

Minimizing $\chi^2(\{a\})$ with respect to the PDF model parameters $\{a\}$ is equivalent to minimizing $\chi'^2(\{a\}, \{r\})$ with respect to both $\{a\}$ and $\{r\}$. This procedure provides a much more streamlined way to obtain the best PDF fit. This formalism, quoted in the main text as Eq. (2.1), forms the basis of our global analysis.

Assuming the measurements D_i , α_i and β_{ki} are in accord with normal statistics, the χ^2 function defined by Eq. (B.5) (or (B.2)) should have a standard probabilistic interpretation for a chi-squared distribution with N_e degrees of freedom, for each experiment.

B.2 Useful tools for evaluating fits and interpreting results

Even when the real experimental errors do not behave in the textbook manner, as is often the case, the formalism developed above provides useful tools for evaluating the quality of the fits and interpreting their results. It also provides hints on reasonable ways to deal with less-than-ideal cases. We describe some of these tools which are used in the presentation of our fit results throughout this paper, and in the error analyses to be discussed in subsequent sections.

First, for any fit, Eq. (B.3) provides a best estimate of each of the systematic errors $\{r_k, k = 1 \dots, K\}$, which we shall denote by $\{\hat{r}_k\}$. For each k , the parameter \hat{r}_k should be of order 1, because the probability for \hat{r}_k to be $\gg 1$ by a random fluctuation is small. If any \hat{r}_k turns out to be noticeably large, the estimate of the systematic errors $\{\beta_{ki}\}$ is suspect.

Second, once the parameters that minimize the χ^2 functions have been determined, we can streamline the comparison of the fit with data—thus evaluate the quality of the fit—by rewriting Eqs. (B.2) and (B.5) as follows:

$$\hat{\chi}^2 \equiv \chi^2(\{\hat{a}\}) = \chi'^2(\{\hat{a}\}, \{\hat{r}\}) = \sum_{\text{expt.}} \left[\sum_{i=1}^{N_e} \frac{(\hat{D}_i - T_i)^2}{\alpha_i^2} + \sum_{k=1}^K \hat{r}_k^2 \right], \quad (\text{B.6})$$

where $\{\hat{a}\}$ (like $\{\hat{r}\}$ above), are the PDF parameters $\{a\}$ at the χ^2 minimum, and

$$\hat{D}_i \equiv D_i - \sum_{k=1}^K \hat{r}_k \beta_{ki}, \quad (\text{B.7})$$

are the data points adjusted by the systematic errors that give rise to the best fit.

Equation (B.6) has the simple appearance of the naive χ_0^2 function (B.1); but it is precise. We note: (i) The systematic shifts of the data points associated with the fit are absorbed into $\{\widehat{D}_i\}$. (ii) The denominator α_i^2 consists of uncorrelated errors only. (iii) The additional (last) term on the right-hand side is just a “constant” when we compare the fit with data, since it is independent of the index i . When the theory curves (obtained from $\{T_i\}$) are compared to the adjusted data points $\{\widehat{D}_i\}$ to assess the goodness-of-fit, one can regard the uncorrelated errors α_i as the *only* measurement error—clearly a great simplification because these errors are random. Figures prepared in this way will give a much more truthful picture of the quality of the fit than comparing theory directly with $\{D_i\}$, since effects due to the unseen correlated systematic errors are impossible to visualize.

B.3 Error analysis of DIS data

The DIS experiments form the bedrock of global analysis of parton distributions. It is seen in Table 1 that the BCDMS and H1 data are within normal statistical expectations, having $\chi^2/N \sim 1$. The ZEUS data have a marginally larger-than-expected χ^2/N , of 267/229. For 229 data points, the probability that $\chi^2 \geq 267$ is 0.063. The NMC data has a much larger χ^2/N of 305/201. This corresponds to a nominal probability of very small magnitude indeed— 3.1×10^{-6} . (This fact was first observed in an early GKK study [47].) It is important to understand the reasons for these numbers and to determine whether the fit to these data sets is acceptable. In addition, in order to assess the uncertainty range of the global analysis, we will need to adopt some uniform procedure for evaluating probabilities among the experiments (cf. Sec. B.4). To both these ends, it is useful to look a little deeper into the χ^2 values for the individual experiments, utilizing the tools developed in the two preceding subsections. We use ZEUS as the first example, since its χ^2 value is at the boundary of being “normal”.

ZEUS data on $F_{2p}(x, Q^2)$: Figure 3 in Sec. 3.1.1 shows the CTEQ6M $F_{2p}(x, Q^2)$ (solid curves) compared to the ZEUS data (corrected by the systematic errors determined by the fit). As noted there, the agreement between theory and data looks quite good. In order to understand the larger-than-expected χ^2 value mentioned above, we need to look deeper. Some insight is provided by Fig. 18. Part (a) of this figure shows a histogram of

$$\Delta_i \equiv \frac{\widehat{D}_i - T_i}{\alpha_i} \tag{B.8}$$

for the ZEUS data. The curve is a Gaussian of width 1 with integral equal to $N = 229$, the number of data points. This histogram is the so-called “pull distribution”—the difference between data and theory in units of the statistical error. The experimental fluctuations seen in Fig. 18a appear (i) Gaussian, (ii) peaked near 0, and (iii) of the normal width. Considering that there are 10 different sources of systematic errors, this test of statistical consistency gives some confidence in the fit.

Next, we note that the net shifts of the data points due to systematic errors are significant, but within the range expected by normal statistics. This is shown in Fig. 18b, which is similar to Fig. 18a but *without* correcting the data points for systematic errors.

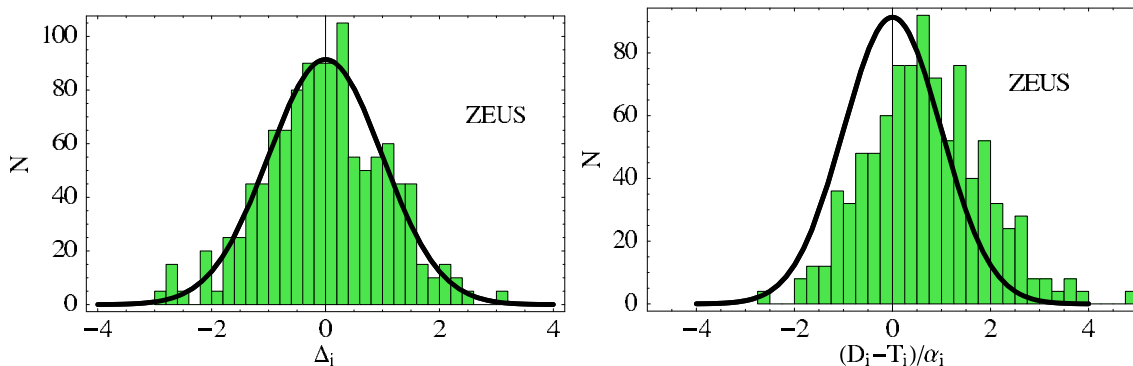


Figure 18: (a) Histogram of Δ_i in Eq. (B.8) for the ZEUS data. The curve is a Gaussian of width 1. (b) A similar comparison but without the corrections for systematic errors on the data points.

A displacement of $\lesssim 0.5$ units in Δ is clearly seen, but that is not unreasonably large. A detailed account of the corrections $\{\hat{r}_1, \hat{r}_2, \dots, \hat{r}_K\}$ (with $K = 10$ for this ZEUS data set) is shown in the following table:

k	1	2	3	4	5	6	7	8	9	10
\hat{r}_k	1.67	-0.67	-1.25	-0.44	-0.00	-1.07	1.28	0.62	-0.40	0.21

Assuming that each systematic error has a Gaussian distribution with the published standard deviation, the probability distribution of r_k should be $P(r) = e^{-r^2/2}/\sqrt{2\pi}$. None of the corrections listed in the table is far outside this distribution. We conclude that the global fit is consistent with the experimental systematic errors, and the corrections calculated from Eq. (B.3) are reasonable.

NMC data on $F_2(x, Q^2)$ from μp scattering: The comparison of NMC data on $F_2(x, Q^2)$ to the CTEQ6M fit has been shown in Fig. 4b, Sec. 3.1.1. Data and theory appear to be in general agreement—there are no systematic patterns of deviation. However, there are clearly outlying points, showing large point-to-point fluctuations of individual data points around the smooth theory curves. To quantify this observation, we again examine the pull distribution for this data set, shown in Fig. 19 in the same form as Fig. 18 for the ZEUS data. Figure 19a shows that (i) the measurement fluctuations appear fairly Gaussian, (ii) the distribution is peaked around $\Delta = 0$, but (iii) the width of the actual histogram appears broader than the normal distribution—there is an excess in outlying (large fluctuation) points, and a corresponding depletion in central (small fluctuation) points.

Given the larger-than-normal fluctuations, how do the systematics of the fit measure up? Comparing Fig. 19a and Fig. 19b, which shows the fluctuations of the uncorrected data, indicates that the net shift in Δ due to systematic errors is ~ 0.3 , which is quite reasonable. The separate shifts associated with the 11 distinct systematic errors for this fit are:

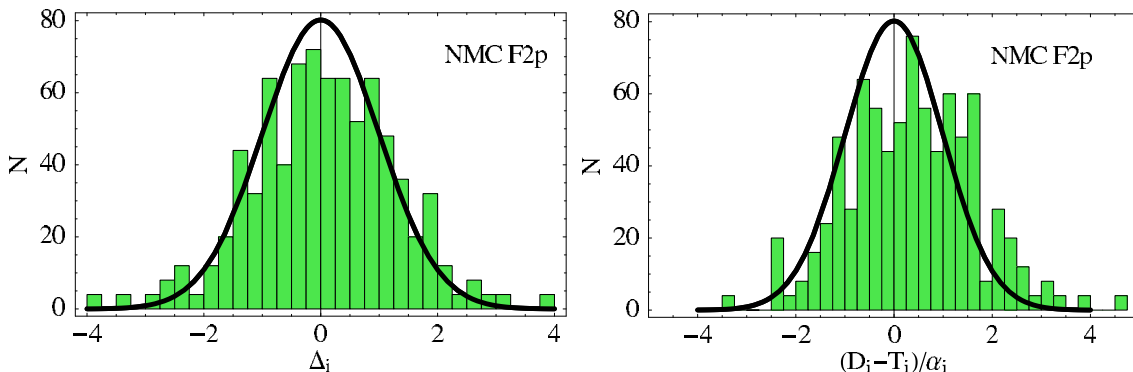


Figure 19: (a) Histogram of Δ_i in Eq. (B.8) for the NMC data. (b) A similar comparison but without the corrections for systematic errors on the data points.

k	1	2	3	4	5	6	7	8	9	10	11
\hat{r}_k	0.67	-0.81	-0.35	0.25	0.05	0.70	-0.31	1.05	0.61	0.26	0.22

We see that the individual deviations are all reasonable, just like the case for ZEUS.

The size of the fluctuations of the data points has very little to do with the viability of the theory model—the excess χ^2 due to such fluctuations cannot be reduced by any improvement in the theory which produces smooth predictions. The quality of the fit is tied much more closely with the systematics, which appear quite normal in the above comparison. As observed before, in Sec. 3.1.1, the most noticeable fluctuations for the NMC data—points with almost the same (x, Q) values—are from data sets taken at different incoming energies. (They can be resolved experimentally, as in the combined data set [21] which we do not use.) For these reasons, we consider the fit to the NMC data to be acceptable.

This example vividly illustrates the usefulness of the method of error analysis adopted here, compared to the traditional one based on the covariance matrix. Equation (B.6) and the plots based on it that we have shown allow a separate examination of the contributions to χ^2 from correlated and uncorrelated errors, which is useful for a more informed assessment of the quality of the fit. The traditional approach, dealing only with the overall χ^2 , can be rather limiting when the experimental errors do not conform to the ideal distributions.

B.4 The tolerance criterion

In this section, we describe the procedure to calculate the range of uncertainty for the parton distributions. In the Hessian approach we adopt, this range is characterized by an overall tolerance parameter, T , that specifies the acceptable neighborhood around the global χ^2 minimum in the parton parameter space by the condition $\Delta\chi^2 < T^2$. Uncertainties of the PDF's and their physical predictions are all linearly proportional to T . We arrive at a quantitative estimate of T by examining the range of overall χ^2 along each of the eigenvector directions within which a good fit to all data sets can be obtained, and

then “averaging” the ranges over the 20 eigenvector directions. The range of acceptable fits along a given direction is estimated by combining the constraints placed on acceptable fits by each individual experiment included in the fit, as described below.

A key feature of this method (which makes the entire approach practical and reliable) is the use of an orthonormal basis in the parton parameter space. An important consequence is that the constant χ^2 hypersurfaces are simple spheroids. It comes as no surprise, then, that when we carry out the mapping of the allowed ranges along the different eigenvector directions, we find that they have the same order of magnitude, so that the averaging of the results to obtain an overall T estimate makes sense. For this reason, we do not need to show the details for all 20 eigenvector directions.

Let us consider the direction of Eigenvector 4 as an example. Consider points along this direction in the neighborhood of the global minimum, labelled by D , the distance from the minimum. These points are candidate fits. We first evaluate the acceptable ranges of fits with respect to the *individual* experiments, according to the known experimental uncertainties. For experiment (e), the individual χ^2 function, χ_e^2 , is a quadratic function of D with minimum at some value D_e . Following Ref. [12] (Sec. 4.1), we define the range of fits acceptable with respect to experiment (e) by finding the upper and lower bounds of D —denoted by D_e^\pm —using the criterion

$$\int_0^{\chi_e^2(D_e^\pm)} P(\chi^2, N_e) d\chi^2 = 0.9 \quad (\text{B.9})$$

where $P(\chi^2, N_e)$ is the standard χ^2 -distribution for N_e data points. The ranges for the individual experiments obtained this way, each shown as a line with the minimum of $\chi_e^2(D)$ marked by a dot, are displayed in Fig. 20. For Eigenvector 4 we see that the strongest bounds on D come from the data sets H1a (low Q H1 data) and BCDMSd (BCDMS deuteron target) on the negative D side, and from the data sets CCFRF3 (CCFR measurements of F_3) and ZEUS on the positive D side.

A practical problem must be resolved in producing the results shown in Fig. 20: how does one obtain meaningful, and reasonably uniform, estimates of the acceptable ranges for the various experiments when the values of χ^2/N vary considerably among the data sets—and in both directions, above and below the canonical value of 1.0? (Cf. Table 1.) In the preceding subsection, we considered some experiments with larger-than-normal values of χ^2/N . The investigations there suggest that the deviations from normal statistical expectations can be attributed mainly to unexplained fluctuations. In order to obtain the acceptable ranges for the individual experiments in a uniform way, it is reasonable to calculate the bounds D_e^\pm for experiment e using the renormalized variable $\chi_e^2/[\chi_e^2(0)/N_e]$, assuming that it obeys a chi-squared distribution with N_e degrees of freedom. Here $\chi_e^2(0)$ is the χ^2 of experiment e for the standard fit S_0 . This procedure provides a pragmatic and uniform way to deal with the problems of acceptability and compatibility among the experimental input encountered in the global analysis. It is often used in other situations involving reconciling data from different experiments [28].

Eigenvector 4 was chosen for illustration purposes. The other cases are similar. Figure 21 shows results for the uncertainty ranges of the experiments along a different direction

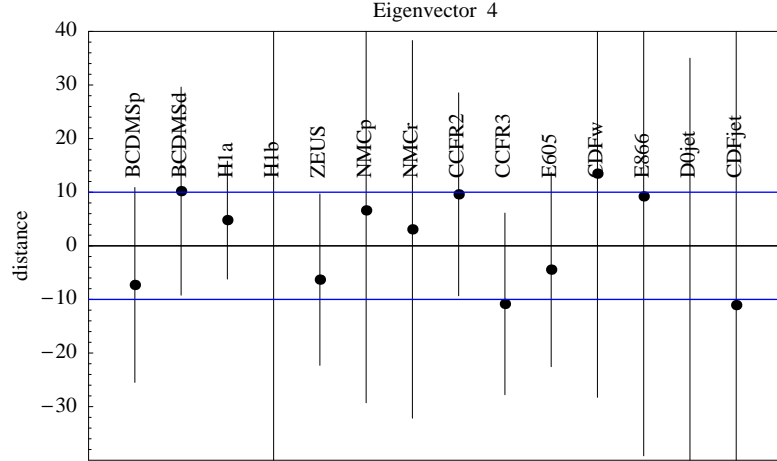


Figure 20: Uncertainty ranges (vertical lines) for the input experiments along the Eigenvector 4 direction. The horizontal lines indicate the *tolerance* T , as discussed in the text.

in the parton parameter space—that of Eigenvector 18. In this case the strongest bounds on the displacement come from the DY and jet experiments.

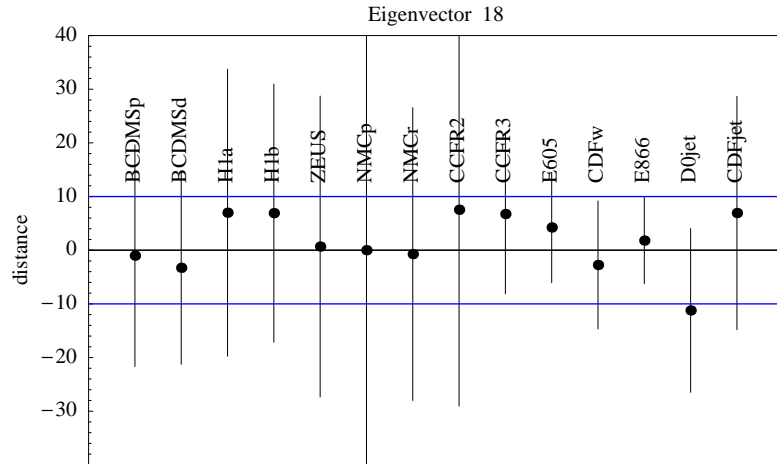


Figure 21: Same as Fig. 20, except for Eigenvector 18.

The next problem is to convert the individual ranges in Fig. 20 or Fig. 21 into a single uncertainty measure. There is no unique way to do this, because the individual ranges shown in these plots are not statistically independent—the candidate fits along the eigenvector direction are all obtained by global fits to the full set of experimental input. In practice, we estimate the overall acceptable range along each eigenvector direction by using the two most restrictive experimental constraints on either side of the minimum. In this way, we obtain the bounds $|D| \sim 10$ for both Eigenvector 4 and Eigenvector 18, indicated by the horizontal lines in Fig. 20 and Fig. 21. Note that these bounds come from different experiments, since the eigenvector directions are sensitive to different features of

the parton distributions.

The above procedure for estimating the uncertainty of D was previously used in [12] to estimate the uncertainties of specific physical predictions (such as cross sections at the Tevatron and LHC colliders), using the Lagrange multiplier method. Each physical variable corresponds to a definite direction in the parton parameter space. The two examples shown above, along two eigenvector directions, are typical for all the directions. Thus, an overall estimate for the tolerance of $T = 10$ follows, as an “average” over all directions in the parton parameter space. This T corresponds to a range of variation of the global χ^2 of $\Delta\chi^2 = T^2 = 100$.

Representing the uncertainties of PDF’s and their physical predictions by one single number T is clearly an oversimplification; it can only be approximate. But given the complexity of the problem, it should be equally clear that attempting to be more precise than this would be rather unrealistic at this stage. In addition to the practical (hence imprecise) measures that need to be adopted to deal with the diverse experimental data sets with nonuniform error specifications, there are additional theoretical uncertainties not yet included in the analysis because they are not easily quantified. In spite of these shortcomings, however, this method of estimating uncertainties is far more systematic and quantifiable than the *ad hoc* procedures that have been used in the past. The important point is that this method, based on the established Hessian formalism, is fundamentally sound; its current limitations are due to compromises in implementation necessitated by experimental realities. The implementation can be systematically improved as both experimental and theoretical input improve with time.

As already noted, the estimated tolerance of $T = 10$ contains experimental uncertainties only. Uncertainties of theoretical or phenomenological origin are not included because they are difficult to quantify. They might be significant. For instance, we have seen throughout this paper that the parametrization of nonperturbative PDF’s has a big influence on the results. Therefore in physical applications the criterion $T = 10$ must be used with awareness of its limitations.

C. Study of Higher Twist Effects

This appendix addresses the question whether it necessary to include higher-twist contributions in the global analysis. It provides the background study that leads to the conclusion mentioned in Sec. 3.3.2, that, with the kinematic cuts to data included in our global analysis, higher-twist terms are not needed.

There have been several studies of the effects of higher-twist (HT) contributions, or power-law corrections, to $F_2(x, Q^2)$ [4, 5, 39, 40]. These usually place some emphasis on describing data in the small- Q range (say, $1 \text{ GeV} < Q < 2 \text{ GeV}$) where higher-twist effects are expected to be noticeable. In the global analysis of PDF’s, the emphasis is different: in order to reliably extract the *universal* parton distributions, it is desirable to focus on the twist-2 sector of PQCD, without the complications of any process-dependent (and model-dependent) effects, such as HT. Thus, we adopt kinematic cuts of $Q > 2 \text{ GeV}$ and $W > 3.5 \text{ GeV}$ to minimize HT effects. The question then becomes whether these kinematic

cuts are sufficient to render HT effects numerically insignificant.²⁰ This question can only be answered phenomenologically by investigating whether the inclusion of HT terms in the theory model is needed to achieve a satisfactory fit, and whether the added degrees of freedom lead to a statistically significant improvement in the fit.

To perform this study, we compare the results of our standard fits with those including HT effects. The model adopted for the higher-twist term is similar to that used in the literature [4, 5, 39, 40],

$$F_2(x, Q^2) = F_2^{NLO}(x, Q^2) \left(1 + \frac{H(x)}{Q^2} \right) \quad (\text{C.1})$$

where

$$H(x) = h_0 + h_1x + h_2x^2 + h_3x^3 + h_4x^4. \quad (\text{C.2})$$

The five parameters $\{h_0, \dots, h_4\}$ are determined by minimizing χ^2 , along with the other model parameters. For simplicity, and following the earlier higher-twist studies, we have assumed that $\{h_0, \dots, h_4\}$ are the same for all DIS processes.

The table below shows the results of our higher-twist study. The first column is the standard fit CTEQ6M, with no higher twist, i.e., $h_k = 0$. The second column is the best fit with higher-twist corrections. The global χ^2 is slightly lower with the higher-twist correction (as it must be, since there are more parameters in this fit), but the reduction $\Delta\chi^2 = -23$ (with 5 extra parameters) does not represent a real improvement of the fit (considering our adopted tolerance). The table also lists the values of χ^2/N for individual DIS experiments.

	CTEQ6M	Higher-twist fit
χ^2	1954	1931
	χ_e^2/N_e	
BCDMS proton	1.11	1.07
BCDMS deuteron	1.11	1.03
H1 A	0.95	0.94
H1 B	1.02	1.02
ZEUS	1.15	1.15
NMC	1.52	1.50

Note that the reduction of χ^2 from inclusion of higher twist, comes mainly from an improved fit to the BCDMS data on μp and μd DIS. The HERA experiments are not affected by the higher-twist correction, as one would expect. The NMC experiment, which, like BCDMS, has data points at low values of Q , is fit only slightly better by including the higher-twist factor $H(x)$. Figure 22 is a graph of the optimal function $H(x)$. It is qualitatively similar to that found in previous studies.

Because the NMC data has a large χ^2 per point compared to other DIS experiments, we have also studied whether a higher-twist function $H_{\text{NMC}}(x)$ can be found that would

²⁰One would like to keep the kinematic cuts as low as is practical, in order to include as much high-statistics data as possible (at relatively low Q) in the global analysis.

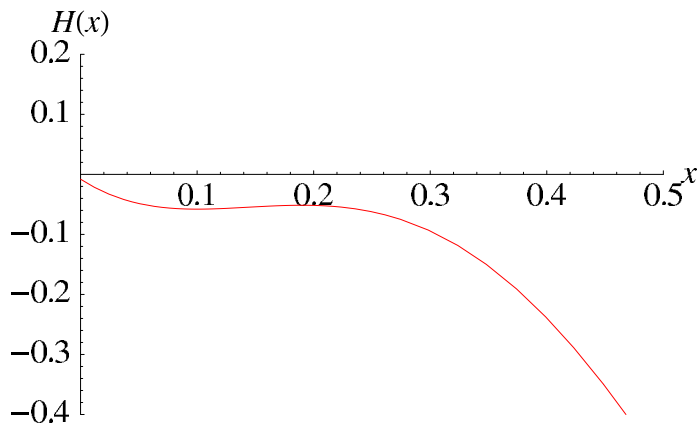


Figure 22: The function $H(x)$ for the phenomenological higher-twist correction to DIS.

significantly reduce the value of χ^2/N for the NMC experiment. The best fit for the NMC data, keeping the PDF's unchanged but optimizing the higher-twist correction to the NMC data, has $\chi^2/N = 1.37$. The associated function $H_{\text{NMC}}(x)$ is somewhat different from the best global $H(x)$ —more strongly negative for $x < 0.5$. However, this “best fit” for NMC causes substantial increase in the χ^2 's of the other DIS experiments—the total χ^2 increases (from 1954 for CTEQ6M) to 2232. Thus, introducing HT contributions does not solve the apparent problem of larger-than-normal χ^2 for the NMC experiment in the global fit. This is not surprising, considering our relatively large cut in the minimum value of $Q^2 = 4 \text{ GeV}^2$.

D. Study of Parametrizations

We have noted in Secs. 2.5, 3 and 5.2 that parametrization of the nonperturbative QCD PDF's now has an important bearing on the results of the global analysis, given the much improved experimental constraints and the newly developed theoretical methods. We have rather extensively explored the influence of parametrization, using the functional forms described in Sec. 2.5 and the iterative Hessian eigenvector method for matching the degrees of freedom in the parametrization with applicable experimental constraints (cf. Sec. 3.2).

Even with tools like these, the choice of parametrization still ultimately involves subjective (i.e., physical) judgements. In this appendix, we shall give only one example of the studies we have carried out, relating to the behavior of the gluon distribution at both small and large x , as discussed in Sec. 3.2.1 and Sec. 5.2.

This study was motivated by an attempt to understand the results of CTEQ6 fits described in Sec. 3 in light of two issues raised by [13]: (i) Do the recent HERA data imply a negative gluon distribution at small x at the scale $Q = 1 \text{ GeV}$? (ii) Do good fits to the new $D\bar{O}$ jet data necessitate an artificial-looking humped structure of the gluon at large x at low Q ? The seeming contradiction between the observations of [13], which give rise to these questions, and the apparent good all-around CTEQ6 fits is resolved by this exercise.

First, the observations of [13] were confirmed when we performed a global fit using the MRST2001 functional form for the gluon, but keeping our parametrization of the quark

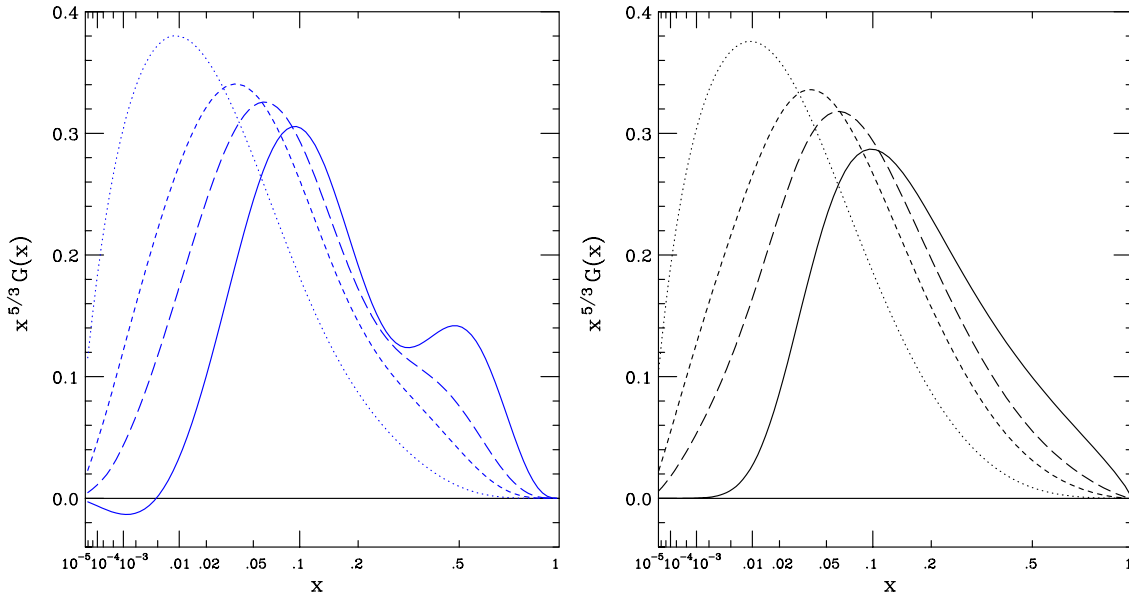


Figure 23: (a) The gluon distribution at $Q = 1, 2, 5, 100$ GeV obtained from a global fit using the MRST functional form for the initial gluon; (b) for comparison, the same gluon distributions from the CTEQ6 parametrization with $Q_0 = 1$ GeV.

degrees of freedom, and fitting to our full set of data with our definition (B.5) for the global χ^2 . Figure 23a shows the resulting gluon distribution at $Q = 1, 2, 5, 100$ GeV. At the scale $Q = 1$ GeV, both the negative gluon at small x and the humped structure at large x found by the least- χ^2 MRST2001J fits are reproduced. For comparison, Figure 23b shows the same distributions from a fit using our parametrization. (To make the comparison possible, this fit was done with $Q_0 = 1$ GeV in place of the CTEQ6 value $Q_0 = 1.3$ GeV.) In this case, there is only a slight shoulder at large x for $Q = 1$ GeV, and the distribution has become completely smooth by $Q = 2$ GeV. Hence the hump structure seen by MRST is an artifact of the particular choice of the parametrization. The gluon distribution is constrained to be positive definite in this parametrization. These two fits differ in overall χ^2 by an amount that is less than our tolerance estimate, so we do not find convincing evidence for a negative gluon distribution even at the very low scale of $Q = 1$ GeV, where the parton distributions are ambiguous anyway because of higher-order and higher-twist corrections.

Since there is no firm theoretical requirement for a positive-definite gluon distribution at Q as low as 1 GeV, we also tried an alternative parametrization for the gluon in which the CTEQ6 functional form is multiplied by an additional factor $(1 + A_6/x)$ that allows $G(x, Q_0)$ to go negative at small x . The resulting gluon distributions are shown in Fig. 24a. This fit has one more fitting parameter, and hence it results in a slightly lower overall χ^2 than CTEQ6M, but the reduction is well within our tolerance range. An interesting feature of this fit is, of course, that it does become negative at $Q = 1$ GeV. But, like the case in Fig. 23a, the distribution rapidly becomes positive under QCD evolution. No trace of the

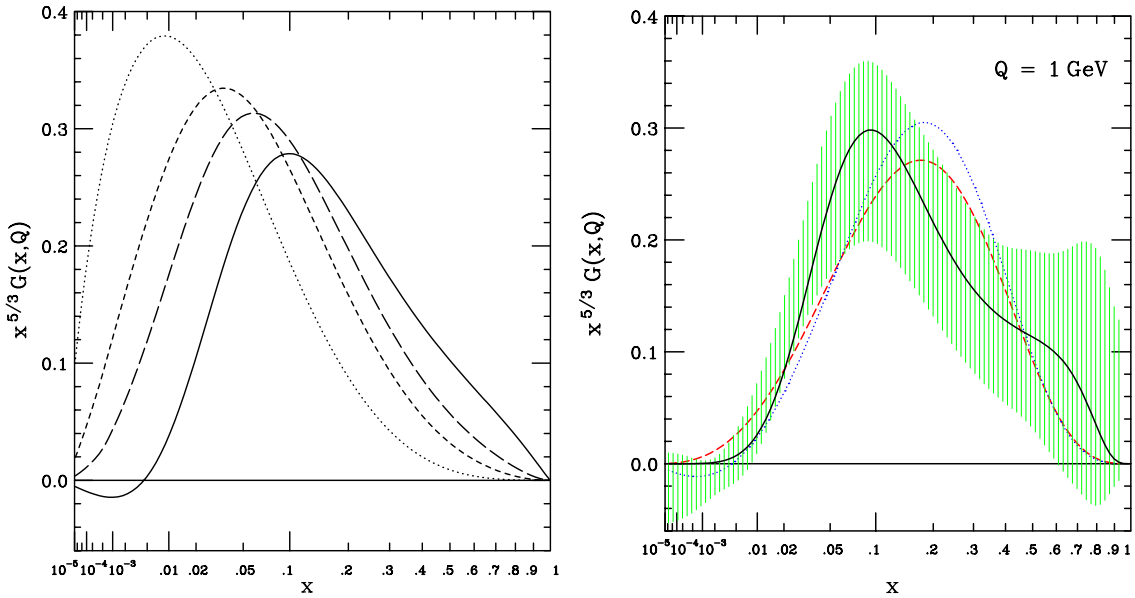


Figure 24: (a) The gluon distribution at $Q = 1, 2, 5, 100$ GeV obtained from a global fit in our parametrization, but allowing for negative gluon at small x . (b) Gluon uncertainty band at $Q = 1$ GeV, covering both + and - regions; dashed: CTEQ5, dotted: MRST2001.

negative region is seen at $Q = 2$ GeV. Is the seeming preference for a negative gluon at $Q = 1$ GeV physically significant? We can answer this question quantitatively by mapping out the range of uncertainty of the gluon distribution at $Q = 1$ GeV using the Hessian method. The result is shown in Fig. 24b. The range of uncertainty, given current experimental constraints, is very large at the $Q = 1$ GeV scale, and it covers both positive and negative territories at small x , as well as large x ! Due to the nature of QCD evolution, the uncertainty decreases rapidly with increasing Q , as shown in Fig. 25.

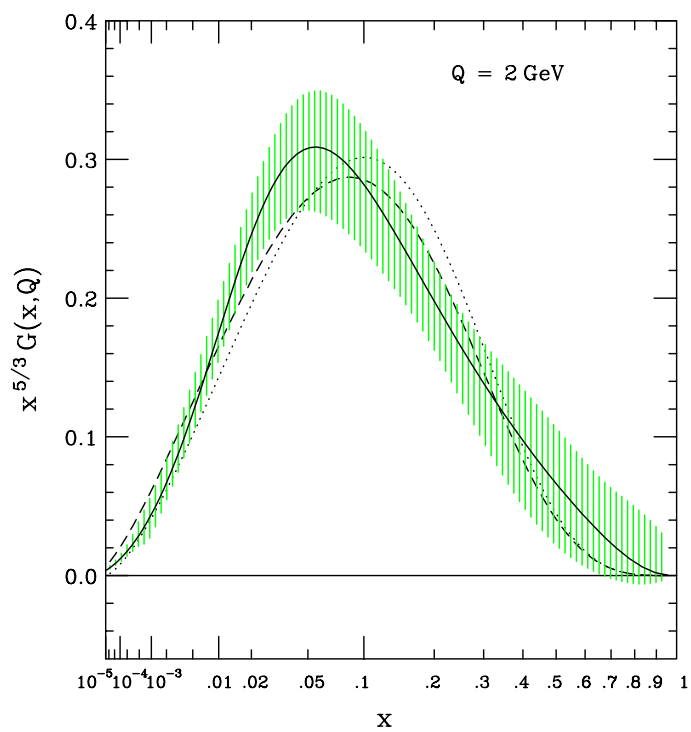


Figure 25: Gluon uncertainty band at $Q = 2 \text{ GeV}$. Same format as Fig. 24.

References

- [1] MRST Analyses: A. D. Martin, R. G. Roberts, W. J. Stirling and R. S. Thorne, Eur. Phys. J. **C 4** (1998) 463 [hep-ph/9803445]; A. D. Martin, R. G. Roberts, W. J. Stirling and R. S. Thorne, Eur. Phys. J. **C 14** (2000) 133 [hep-ph/9907231].
- [2] CTEQ Analyses: J. Botts *et al.*, Phys. Lett. **B 304** (1993) 159 [hep-ph/9303255]; H. L. Lai *et al.*, Phys. Rev. **D 51** (1995) 4763 [hep-ph/9410404]; H. L. Lai *et al.*, Phys. Rev. **D 55** (1997) 1280 [hep-ph/9606399]; H. L. Lai *et al.*, Eur. Phys. J. **C 12** (2000) 375 [hep-ph/9903282].
- [3] M. Gluck, E. Reya and A. Vogt, Z. Phys. **C 67** (1995) 433; and Eur. Phys. J. **C 5** (1998) 461 [hep-ph/9806404].
- [4] S. I. Alekhin, Eur. Phys. J. **C 10** (1999) 395 [hep-ph/9611213]; hep-ex/0005042; and Phys. Rev. **D 63** (2001) 094022 [hep-ph/0011002].
- [5] M. Botje, Eur. Phys. J. **C 14** (2000) 285 [hep-ph/9912439].
- [6] V. Barone, C. Pascaud and F. Zomer, Eur. Phys. J. **C 12** (2000) 243 [hep-ph/9907512]; C. Pascaud and F. Zomer, Tech. Note LAL-95-05.
- [7] W. T. Giele and S. Keller, Phys. Rev. **D 58** (1998) 094023 [hep-ph/9803393]; W. T. Giele, S. A. Keller and D. A. Kosower, [hep-ph/0104052].
- [8] W. Bialek, C. G. Callan and S. P. Strong, Phys. Rev. Lett. **77** (1996) 4693; V. Periwai, Phys. Rev. **D 59** (1999) 094006 [hep-ph/9912439].
- [9] R. D. Ball, in *Proceedings of the XXXIVth Rencontres de Moriond*, 1999.
- [10] J. Pumplin, D. R. Stump and W. K. Tung, Phys. Rev. **D 65** (2002) 014011 [hep-ph/0008191].
- [11] J. Pumplin *et al.*, Phys. Rev. **D 65** (2002) 014013 [hep-ph/0101032].
- [12] D. R. Stump *et al.*, Phys. Rev. **D 65** (2002) 014012 [hep-ph/0101051].
- [13] A. D. Martin, R. G. Roberts, W. J. Stirling and R. S. Thorne, hep-ph/0110215.
- [14] H1 Collaboration: C. Adloff *et al.*, Eur. Phys. J. **C 13** (2000) 609 [hep-ex/9908059]; Eur. Phys. J. **C 19** (2001) 269 [hep-ex/0012052]; Eur. Phys. J. **C 21** (2001) 33 [hep-ex/0012053].
- [15] ZEUS Collaboration: S. Chekanov *et al.*, Eur. Phys. J. **C 21** (2001) 443 [hep-ex/0105090]; A.M. Cooper-Sarkar, Proceedings of International Europhysics Conference on HEP 2001, Budapest [hep-ph/0110386].
- [16] DØ Collaboration: B. Abbott *et al.*, Phys. Rev. Lett. **86** (2001) 1707 [hep-ex/0011036]; and Phys. Rev. **D 64** (2001) 032003 [hep-ex/0012046].
- [17] E866 Collaboration: R. S. Towell *et al.*, Phys. Rev. **D 64** (2001) 052002 [hep-ex/0103030].
- [18] CCFR Collaboration: U. K. Yang *et al.*, Phys. Rev. Lett. **86** (2001) 2742 [hep-ex/0009041].
- [19] BCDMS Collaboration: A. C. Benvenuti *et al.*, Phys. Lett. **B 223** (1989) 485.
- [20] BCDMS Collaboration: A. C. Benvenuti *et al.*, Phys. Lett. **B 236** (1989) 592.
- [21] New Muon Collaboration: M. Arneodo *et al.*, Nucl. Phys. **B 483** (1997) 3 [hep-ph/9610231]; and M. Arneodo *et al.*, Nucl. Phys. **B 487** (1997) 3 [hep-ex/9611022].
- [22] CCFR Collaboration: W. G. Seligman *et al.*, Phys. Rev. Lett. **79** (1997) 1213 [hep-ex/970107].

- [23] E605 Collaboration: G. Moreno *et al.*, Phys. Rev. **D 43** (1991) 2815.
- [24] CDF Collaboration: F. Abe *et al.*, Phys. Rev. Lett. **81** (1998) 5754 [hep-ex/9809001].
- [25] CDF Collaboration: T. Affolder *et al.*, Phys. Rev. **D 64** (2001) 032001 [hep-ph/0102074].
- [26] M. Botje, Proceedings of *New Trends in HERA Physics 2001*, Ringberg Castle, Tegernsee, Germany, 17-22 Jun. 2001 [hep-ph/0110123].
- [27] J. C. Collins and J. Pumplin, hep-ph/0105207.
- [28] Particle Data Group: D. E. Groom *et al.*, Eur. Phys. J. **C 15** (2000) 1.
- [29] M. A. Aivazis, F. I. Olness and W. K. Tung, Phys. Rev. **D 50** (1994) 3085 [hep-ph/9312318]; M. A. Aivazis, J. C. Collins, F. I. Olness and W. K. Tung, Phys. Rev. **D 50** (1994) 3102 [hep-ph/9312319].
- [30] R. S. Thorne and R. G. Roberts, Phys. Lett. **B 421** (1998) 303 [hep-ph/9711223]; Phys. Rev. **D 57** (1998) 6871 [hep-ph/9709442]; and Eur. Phys. J. **C 19** (2001) 339 [hep-ph/0010344].
- [31] A. Chuvakin, J. Smith and W. L. van Neerven, Phys. Rev. **D 61** (2000) 096004 [hep-ph/9910250]; and Phys. Rev. **D 62** (2000) 036004 [hep-ph/0002011].
- [32] M. Cacciari, M. Greco and P. Nason, JHEP **9805** (1998) 007 [hep-ph/9803400].
- [33] W. K. Tung, S. Kretzer and C. Schmidt, Proceedings of *New Trends in HERA Physics 2001*, Ringberg Castle, Tegernsee, Germany, 17-22 Jun. 2001 [hep-ph/0110247].
- [34] M. Dasgupta and G. P. Salam, hep-ph/0110213.
- [35] P. M. Nadolsky and Z. Sullivan, in *Proc. of the APS/DPF/DPB Summer Study on the Future of Particle Physics (Snowmass 2001)* ed. R. Davidson and C. Quigg, hep-ph/0110378.
- [36] S. Kuhlmann *et al.*, Phys. Lett. **B 476** (2000) 291 [hep-ph/9912283].
- [37] U. K. Yang and A. Bodek, Phys. Rev. Lett. **82** (1997) 2467 [hep-ph/9809480].
- [38] J. Huston, S. Kuhlmann, H. L. Lai, F. I. Olness, J. F. Owens, D. E. Soper and W. K. Tung, Phys. Rev. **D 58** (1998) 114034 [hep-ph/9801444]; A. D. Martin, R. G. Roberts, W. J. Stirling and R. S. Thorne, Eur. Phys. J. **C 14** (2000) 133 [hep-ph/9907231]; and [hep-ph/0110215].
- [39] A. D. Martin, R. G. Roberts, J. S. Stirling and R. S. Thorne, Phys. Lett. **B 443** (1998) 301 [hep-ph/9808371].
- [40] S. I. Alekhin and A. L. Kataev, Phys. Lett. **B452** (1999) 402 [hep-ph/9812348].
- [41] CDF Collaboration: F. Abe *et al.*, Phys. Rev. Lett. **77** (1996) 438 [hep-ex/9601008].
- [42] J. Huston, E. Kovacs, S. Kuhlmann, H. L. Lai, J. F. Owens, D. E. Soper and W. K. Tung, Phys. Rev. Lett. **77** (1996) 444 [hep-ph/9511386].
- [43] DØ Collaboration: B. Abbott *et al.*, Phys. Rev. Lett. **82** (1999) 2451 [hep-ex/9807018].
- [44] See, for instance, S. I. Alekhin, Phys. Lett. **B 519** (2001) 57 [hep-ph/0107197].
- [45] See, for example, the writeups in <http://wwwlapp.in2p3.fr/conferences/LesHouches/Houches2001/> and <http://pdf.fnal.gov>.

- [46] J. C. Collins, “Minijets and Regge theory”, in Proceedings of Workshop on SSC physics, UCLA, Jan 1986 (World Scientific, Singapore, 1986); and “Semi-hard processes and QCD”, in Physics Simulations at High Energy (V. Barger, T. Gottschalk, F. Halzen, eds.), (World Scientific, Singapore, 1987).
- [47] D. Kosower, talk given at ‘Les Rencontres de Physique de la Valle d’Aoste’, La Thuile, February 1999.